# Advanced muscle-on-chip devices: Growing muscle project

BSc Thesis

Martijn Leeuwenburg, Rob Krüger & Wybe van der Plas

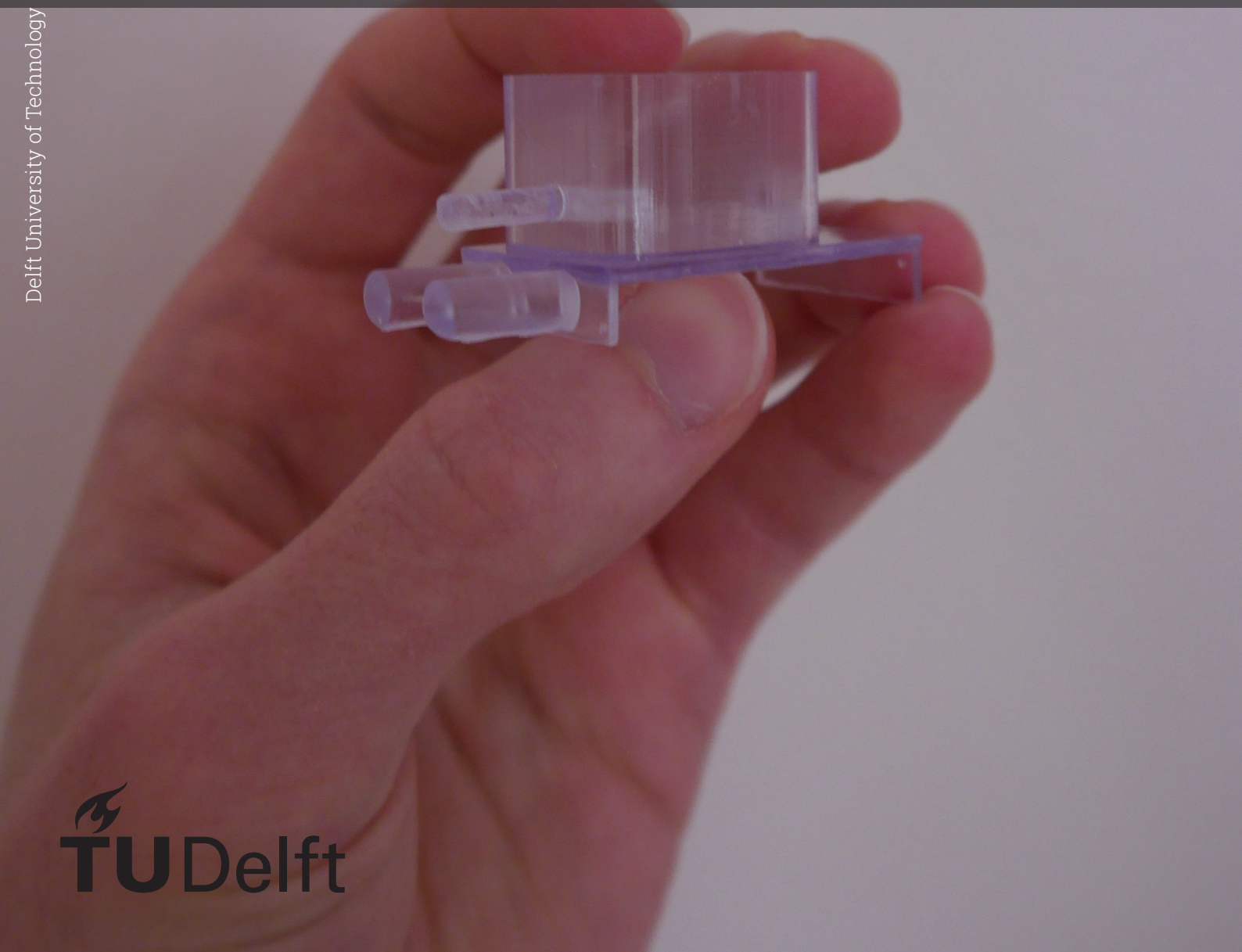

Delft University of Technology

TU Delft

# Advanced muscle-on-chip devices: Growing muscle project

by

Martijn Leeuwenburg, Rob Krüger & Wybe van der Plas

Student Number: 5819148 (Martijn Leeuwenburg)
Student Number: 5780608 (Rob Krüger)
Student Number: 5825334 (Wybe van der Plas)

TU Delft

# Abstract

This report presents the design and implementation of a single-well muscle-on-a-chip device capable of displacing one of the support pillars to which muscle tissue is bound, using an electromechanical actuator. In addition to this displacement capacity, the muscle tissue can be electrically stimulated, allowing for the measurement of corresponding contraction forces via post-deflection methods. Experimental results demonstrate that the actuated support pillar can be moved by approximately $40\mu m$ per step.

# Preface

This thesis is written in the context of the Bachelor Graduation Project for the BSc Electrical Engineering at TU Delft. The project was done in collaboration with Erasmus MC for the goal of enabling them to add a new layer of research to their muscle-on-a-chip devices, as well as add some engineering insight. We would like to thank all the wonderful people at Erasmus MC for allowing us to use their special printing equipment, as well as the continued guidance on design choices. Special thanks go to Federico Silvestri, Alessandro Iuliano, dr. Pim Pijnappel and our supervisor from TU Delft, dr. Massimo Mastrangeli.

*Martijn Leeuwenburg, Rob Krüger & Wybe van der Plas*
*Delft, June 2025*

# Contents


**1 Introduction** **1**
1.1 State of the art . . . 1
1.2 Problem definition . . . 2
1.3 Thesis synopsis . . . 2

**2 Program of requirements** **3**
2.1 Requirements . . . 3
2.1.1 Mandatory Requirements . . . 3
2.1.2 Trade-off Requirements . . . 3

**3 Design Considerations** **4**
3.1 Moving the support pillars . . . 4
3.2 Flexible versus non-flexible support pillars . . . 4
3.3 Stimulation and measuring the contraction force . . . 5

**4 Design of the linear actuator** **6**
4.1 A review on actuators . . . 6
4.1.1 Types . . . 6
4.1.2 Motors . . . 8
4.2 Chosen actuator . . . 12
4.3 Required components . . . 12
4.4 Resolution analysis . . . 13
4.5 Motor casing . . . 14

**5 Design of the well** **15**
5.1 General design decisions . . . 15
5.1.1 Pillar design and connecting to the actuator . . . 15
5.1.2 Well shape and chamber . . . 16
5.1.3 Sealing . . . 17
5.1.4 Lid . . . 17
5.2 Solving the flexible pillar dilemma . . . 18

**6 Electrical subsystem** **20**
6.1 Electrodes . . . 20
6.1.1 Materials and placement . . . 20
6.2 Function generation and amplification . . . 20

**7 Assembly and results** **21**
7.1 UI . . . 21
7.2 Printing and assembly . . . 23
7.2.1 Printing the well . . . 23
7.2.2 Connecting the well and actuator . . . 24
7.3 Results . . . 25
7.3.1 Actuation results . . . 25
7.3.2 Electrical results . . . 26

**8 Discussion and Conclusion** **27**
8.1 Future work . . . 27

**A Individual animation frames** **28**
A.1 Stepper Motor . . . 28
A.2 UI . . . 28

**B Alternate well design** **30**
B.1 About the alternate design . . . . . 30
B.2 Alternate design . . . . . 31

**C Source code** **33**

**References** **34**

# 1 Introduction

Muscle diseases such as Duchenne Muscular Dystrophy (DMD) have long challenged researchers due to the inherent limitations of traditional donor-based studies. Isolated muscle tissue, once removed from its native environment, rapidly loses the dynamic contractility and responsiveness intrinsic to healthy muscle. Consequently, these samples fail to recapitulate the physiological complexity necessary for an accurate study of disease mechanisms.

One promising solution to this research conundrum is the advent of Muscle-on-a-Chip technology. Muscle-on-a-chip devices have revolutionized the way we simulate live muscle behaviour in vitro, enabling not only the electrical stimulation of muscle bundles but also the measurement of contraction forces in a controlled micro-environment. Despite these advances, current platforms typically do not emulate the stretching and elongation that muscles naturally undergo in the human body, a critical factor in both muscle growth and disease progression.

This project seeks to address the problem by introducing a chip design featuring a movable support pillar capable of dynamically stretching the muscle bundle. By integrating mechanical stretching into the muscle-on-a-chip framework, the proposed system better mimics in vivo conditions, thereby offering enhanced insights into muscle development and the pathophysiology of diseases like DMD.

## 1.1. State of the art

The muscle-on-a-chip device is a specialized implementation of an Organ-on-Chip (OOC) system, designed to host an in vitro three-dimensional muscle tissue. These devices are most often employed to test potential new drugs. The 3D solution in general consists of five parts:

1. The muscle cells
2. A medium to provide nutrients to the cells among other functions.
3. Support pillars to give structural support and guide the 3D tissue formation.
4. Biological cues, more often than not electrical stimulation.
5. Measurement techniques, to measure the contractile force of the muscle bundle.

In most designs, the support pillars are provided with a cap, and are made from elastomeric materials [1, 2, 3, 4, 5, 6, 7, 8]. This in turn allows the muscle bundle to pull on the pillar during stimulation. The bending of the pillar can be measured to determine the contraction force of the muscle bundle using a method called post deflection [9]. Post deflection can be done in a variety of ways, such as optical measurements [1, 7, 10, 11], capacitive sensing [6, 12] or optical triangulation [13].

The well in which the muscle tissue grows and the medium can be found, must be kept uncontaminated while placed inside an incubator, to facilitate an unbothered growth of the cells. This requires the need for any parts in contact with the cells and medium to be biocompatible. 3D printed parts are more often than not sterile and can be used to print the well and support pillars [14]. To enclose the well, a

Petri dish is most often used. The lid of a Petri dish often contains spacers, which lift the lid ever so slightly to allow gas exchange. For the biological cues, an electrical contact has to be kept inside the well and medium. These contacts should be corrosion resistant for as much as possible, which in turn increases their biocompatibility [15]. Soldering used to join the electrical contacts and signal generating circuit parts, should also be kept biocompatible. Lead-tin soldering provides good protection against corrosion, but are toxic for the cell environment [16]. Other options include gold-tin soldering, which provides better biocompatibility [17] or covering the soldered joints with epoxy, which provides both corrosion resistance and biocompatibility [18].

In most designs, a plate is used that houses multiple wells at the same time, to allow for multiple muscle tissues to grow alongside each other. The wells typically contain a chamber, in which the muscle tissue and support pillars reside, to direct the cells to the right position and aid the growth of the tissue.

All modern designs still suffer from the fact that the support pillars stay locked in place, which in turn means the muscle tissue has a fixed length and position. Strides have been made to simulate more realistic behaviours for the tissue [19], but these solutions still don't allow for the muscle tissue to grow further in length.

## 1.2. Problem definition

This project should aim to develop a muscle on a chip device, which allows for a displacement of the support pillars, while keeping all other functions of a typical setup intact. This includes electrically stimulating the muscle, in addition to providing a way to measure the corresponding contraction force of the developed muscle bundle. Due to the fact that this project is the first attempt of its kind, it will constrain itself to designing a single well instead of multiple.

## 1.3. Thesis synopsis

The thesis can be summarised as follows. Chapter 2 specifies the requirements that need to be taken into account in the design. Chapter 3 will discuss the main problems to be solved in the project. Chapter 4 and 5 will discuss the design decisions made for the well of the system and its accompanying actuator. Chapter 6 will discuss the electrical system used to stimulate the muscle, after which Chapter 7 will detail the assembly process and give a report on the results of the prototype. Finally, a discussion of the results and a conclusion will be given in Chapter 8.

# 2

# Program of requirements

As described in Chapter 1, the goal of this project was to design and build a system that supports a small muscle bundle to grow between two support points that can be moved apart to accommodate the lengthwise growth of the muscle bundle. In addition, the design should incorporate a subsystem to electrically stimulate this muscle bundle.

This chapter lists the requirements necessary to realise this system, which are subdivided into mandatory and trade-off requirements.

## 2.1. Requirements

### 2.1.1. Mandatory Requirements

1. The design must avoid sharp angles to minimize bacteria growth.
2. The design must allow for 3D printing.
3. The complete system must withstand the temperatures and humidity of an incubator. (Around $37°C$ and $95\%$ humidity.)
4. Materials used for areas in contact with the medium and cells must be biocompatible.
5. All materials must be sterilizable.
6. The environment in the well must be kept separated from the outside world, while still allowing gas exchange.
7. The well must house a chamber for the muscle bundle.
8. The tissue cells must be visible from top to bottom (the well must be see-through.)
9. The system must allow for the growth of the muscle tissue.
10. The muscle must be electrically excitable with a 0-5V square wave.
11. The system must allow the user to increase the distance between the anchor points of the muscle tissue.
12. The muscle bundle must be allowed to contract when it is electrically excited.
13. There must be at least $3mm$ of space available for the muscle to extend.

### 2.1.2. Trade-off Requirements

1. Usage of the product should be kept simple for non-technical users.
2. Material and machinery costs should be kept under €200.
3. The support pillar should ideally be moved in steps of $50\mu m$ or less.

# 3

# Design Considerations

This chapter will detail the most important design challenges faced in the design process of the project, as well as some possible solutions.

## 3.1. Moving the support pillars

The task of displacing the support pillars in a muscle-on-a-chip system requires careful consideration of various design options. One potential solution is manually adjusting the position of the support pillar by attaching it to an external mechanism that could be manipulated outside the well. While this approach offers simplicity in terms of implementation, it fails to provide the necessary accuracy and repeatability required for small-scale, delicate applications such as muscle-on-a-chip systems. Therefore, a more precise and reliable solution is needed.

A promising candidate for this task is the use of linear actuators. Linear actuators are actuators that produce motion along a single axis, while most common motors produce rotary motion. They can be made capable of producing controlled, precise motion, which is ideal for manipulating the support pillar with the necessary accuracy. This characteristic is crucial for ensuring the controlled stretching of the muscle to facilitate its growth and functional simulation.

While commercial linear actuators are widely available, they often come with high costs and limited flexibility in terms of integration within the confined space of the well. Additionally, these off-the-shelf actuators may present challenges in terms of customizability for secure attachment to the support pillar. As a result, a decision was made to design and fabricate a custom linear actuator tailored to the specific needs of this system. Chapter 4 will list some options regarding linear actuation, as well as document the chosen design for the project.

## 3.2. Flexible versus non-flexible support pillars

Currently, research groups often measure the contraction force of the muscle bundle by fabricating one or both support pillars from elastomeric materials [1, 4, 5, 10]. When the muscle contracts during electrical stimulation, it exerts an inward force on the flexible pillar. The pillars deflection is then tracked through optical measurements, allowing researchers to calculate the contraction force. However, the flexibility of the pillar presents a major challenge during the muscle growth phase of the project. If the pillar remains flexible while the muscle stretches, the muscle could inadvertently pull the pillar along its path, displacing the muscle bundle rather than allowing it to stretch properly. In order to combat this issue, there are two main possible solutions that can be used:

1. **Rigid support pillars:** Construct both support pillars from a rigid material. In this way, the muscle cannot move either pillar during the growth phase. This approach requires some other form of measurement technique, or a different approach to the flexible part of the pillar in order to measure the contraction force of the muscle.
2. **One flexible support pillar:** Make at least one of the pillars flexible, but create some system to

stop the flexibility of the pillar during the growth phase.

For this project, the decision was made to explore the first option, due to the way the actuated pillar is shaped in the design. Chapter 5 presents a detailed discussion of the design concepts underlying this solution. Although ideas for the second option were also designed, concerns about the possibility of the muscle bundle sliding off the support pillar made this option unfavourable. In order to preserve some of the efforts from this design, some sketches and an explanation will be included in Appendix B.

## 3.3. Stimulation and measuring the contraction force

As has been discussed in Section 1.1, it is essential to stimulate the muscle tissue within the well to induce contraction. This stimulation is typically done trough the use of electrodes. In previous studies, the chosen electrode material was either steel [2], platinum[5, 20], or carbon[7]. Other materials, such as silver could also be used as electrodes [21]. For the purposes of this project, carbon rods were selected due to their biocompatible properties and cost-effectiveness, making them a practical choice compared to other materials.

Regarding the measurement of the muscle contraction force, the decision was made to retain the elastomeric material in the design of the well. This choice facilitates optical measurement techniques, providing a non-invasive method for monitoring contraction. While other measurement methods, such as strain gauges, could have been implemented, they would require additional subsystems and could shift the focus away from the primary goal of actuating the support pillar. Consequently, the use of elastomeric material aligns better with the project's objectives while simplifying the design.

# 4

# Design of the linear actuator

This chapter will explain the linear actuator used to move the pillar during the growth process. During the design process, emphasis was placed on keeping costs down while keeping a fine enough resolution.

## 4.1. A review on actuators

This section will discuss various types of linear actuators and the design choices made to obtain the actuator used in the prototype.

### 4.1.1. Types

#### Mechanical

Mechanical linear actuators can convert circular motion to linear motion. The original circular motion can come from various sources, such as a human rotating a handle manually or an electromagnetic motor.

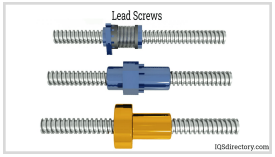


**Figure 4.1:** Three leadscrews with different type of nuts *Image taken from iqsdirectory.com [22]*

The mechanism most often used is that of a lead screw. A lead screw is similar to a threaded rod found in screws and bolts, with their main difference in how the threads are designed. The thread on a screw or bolt is meant to fasten something, while the thread on a lead screw is meant to convert circular motion to linear motion. Therefore, threads on a screw or bolt are designed to maximize friction, to keep it properly fastened, while the threads on a lead screw are designed to minimize friction, to reduce losses during the motion conversion. On the lead screw, a nut is attached. If this nut is then prevented from rotating, turning the lead screw will result in a linear movement for the nut, since it is being pushed by the threads.

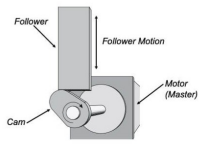


**Figure 4.2:** A simple cam mechanism *Image adapted from tolomatic.com [23]*

A widely used alternative is a cam mechanism. This consists of an irregular shape, such as an ellipse, attached to a rotating shaft. This rotating shaft is then placed in proximity to a ”Cam follower”, which could, for example, be a stud connected to a spring. When the ends of the ellipse make contact with the follower, they push the follower down, creating linear motion. This concept is often used in combustion engines, where a cam mechanism controls the actuation of the intake and exhaust valves, since a cam mechanism allows for periodic linear motion.

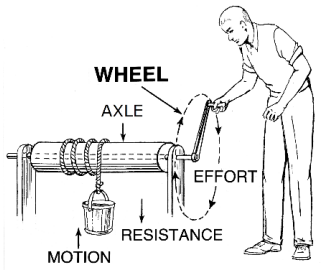


**Figure 4.3:** The wheel and axle system of an old well
*Image taken from energyeducation.ca [24]*

The final mechanism to be discussed is a wheel and axle system. A great example of this mechanism is that of an old well. While some used a pulley system to make it easier to hoist water up, others had a big wooden shaft connected to a wheel. Spun around this shaft was a long rope, and by turning the wheel, the rope would either be unraveled or wound up. Therefore, the circular motion of turning the wheel is converted into linear movement for the bucket. Many other variants of this principle exist, such as a chain drive. Chains are often used to transmit circular motion, thus also delivering circular motion, like in a bicycle, where the chain transmits the circular motion from the pedals to the rear wheel. By fixing something on the chain, however, you get linear movement as long as the chain is properly tensioned. Recently, the same principle but using belts is more popular, since they're easier to manufacture and replace. Another wheel and axle system is that of a rack-and-pinion setup. Here, a circular gear, called the pinion, is connected to a linear gear, also called a rack. When the pinion rotates, its teeth push against the teeth of the rack, resulting in a linear movement for the rack.

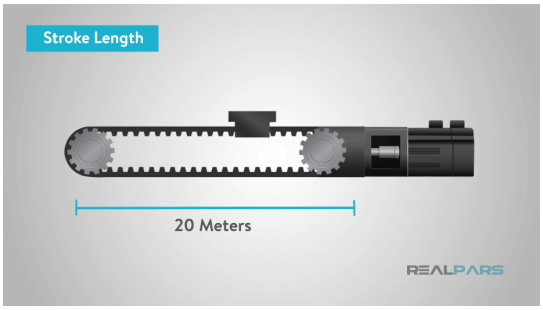


**(a)** Belt
*Image taken from realpars.com [25]*

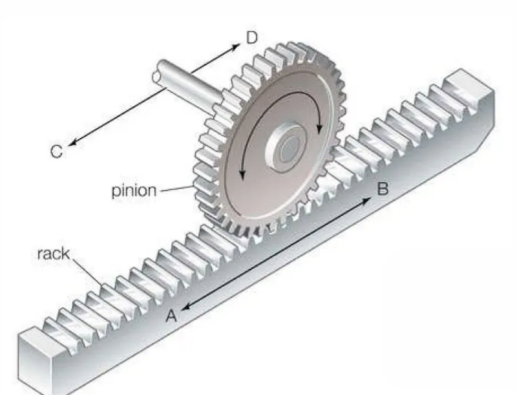


**(b)** Rack and pinion
*Image adapted from theengineeringchoice.com [26]*

**Figure 4.4:** Two specialized wheel and axle systems

### Pressure-based

Another method to achieve linear motion is by using a pressure-based linear actuator. These have two main versions, namely hydraulic actuators and pneumatic actuators. These actuators rely on a pump to increase the pressure inside them, which will generate a force. A hydraulic actuator utilizes liquids, often a specialized oil, while pneumatic actuators work with compressed air. As long as the fluid flow can be accurately monitored, these actuators offer precise control and high-power output, at the cost of a bulky setup and the need for many safety constraints. The bulky setup comes from the need for a hydraulic pump and pressure-resistant components. Since the pressure levels are potentially lethal in case of a small leak, it is also not recommended to use this system with inexperienced people. Pneumatic actuators are less dangerous, but still require a pump, making this type of linear actuator irrelevant for this project.

### Piezoelectric

Some materials exhibit the piezoelectric effect. Because of this phenomenon, an electric charge is generated when mechanical stress is applied to the material, and vice versa. Therefore, when a voltage is applied to a piezoelectric material, the mechanical stress generated will cause the material to deform. Using various mechanisms, this enables the manufacturing of both linear and rotary actuators with great precision because a large difference in applied voltage causes only a small deformation in the material. This does have the consequence, however, that cheap actuators (with prices around €15) can only produce small displacements, in the order of 30 to 100 $\mu m$. Larger displacements are obtainable with complex mechanisms, which also require a dedicated controller, driving up prices to around €1000.

#### Solenoid

The final actuator type worth discussing is the solenoid. These actuators have a coil around a metal plunger. When the coil is energized, it generates a magnetic field that either pulls the plunger inwards or pushes it out. Therefore, solenoid actuators provide cheap and power-efficient linear motion, but lack in position control. The magnetic force produced by the coil is highly nonlinear, and the piston has significant friction. This results in a period after applying a voltage where the piston is unable to overcome the friction, followed by it suddenly starting to move as it overcomes this friction, and ending with the magnetic force increasing substantially as the plunger nears the closing position. This behaviour makes it impossible to accurately control the plunger's position and solenoids working in a binary on/off, or extended/retracted, states.

#### Design choices

| Type | Advantages | Disadvantages |
|---|---|---|
| Lead screw | Compact, minimal wear | Needs a linear rail with appropriate bearings which are expensive |
| Cam mechanism | Periodic movement | Require precision manufacturing |
| Belt driven | Simple, low cost, backlash free | Belts will degrade fast inside an incubator due to heat and humidity |
| Rack and pinion | Simplest, easily 3D printed, stiff | Lower precision due to higher tolerances, needs to be preloaded to eliminate backlash |
| Hydraulic | High power transfer, robust and durable | Complex setup with pumps, valves, and filters, risk of leaks |
| Pneumatic | Fast actuation, safe | Air is compressible, so poor position control. Requires an air compressor running at all times. |
| Piezoelectric | Extremely precise movement | Highly expensive compared to other options for appropriate displacement distances. |
| Solenoid | Cheapest, fast actuation, no maintenance | Require sensors for position control, which will still be inaccurate compared to other mechanisms. |

**Table 4.1:** Table discussing the advantages and disadvantages of every mechanism.

*Backlash is caused by play in the mechanism, allowing for small movements while the actuator should be stationary.*

From this table, it was chosen to use a rack-and-pinion setup for the prototype. This decision comes primarily from the fact that it is mechanically one of the simplest mechanisms, requiring only a gear, a rack, and a rail to guide the rack. Since the prototype will be 3D printed, the guide rail can also be 3D printed, while a metal rack would require bearings or lubrication. This printed guide rail will still wear, but it was chosen to focus on a proof-of-concept and ignore wear for now. A piezoelectric actuator would have been chosen if cost was not a constraint, because of their superior resolution for small displacements.

### 4.1.2. Motors

In Section 4.1.1 - Design Choices, it was chosen to use a mechanical mechanism. Therefore, an appropriate motor must be selected to drive the gear. This section will explore various electromagnetic motor options. Since AC motors are generally not found in small sizes and are more difficult to accurately control, this section will focus only on DC motors.

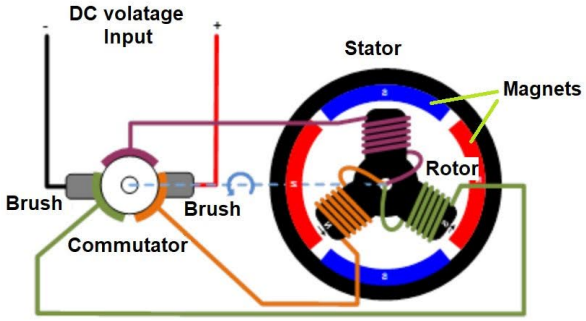


**Figure 4.5:** Schematic showing the permanent magnets, coils and brush inside a brushed DC motor
*Image taken from firgelliauto.com [27]*

### DC motors

Brushed and brushless are two of the most common DC motor types. Both contain permanent magnets that generate a magnetic field and coils wound around an iron core. The placement of these magnets and coils, however, differs per type.

### Brushed DC motor

In a brushed DC motor, the magnets are placed on the stator, generating a stationary magnetic field. The coils are then placed on the rotor, which is free to rotate. When a current is fed through these coils, they will also generate a magnetic field. This magnetic field causes the coils to be repelled or attracted by the permanent magnets, causing the rotor to rotate. However, after only half a rotation, the poles of the coils and the permanent magnets will be aligned in such a way that there are no attracting or repelling forces generated anymore, and the motor will stall. At that moment, the current needs to be reverted, which is done automatically mechanically with brushes, hence the name brushed DC motor. These brushes are fixed to the stator and will not move during operation. The commutator, attached to the rotor, consists of segmented contacts, one for each coil, and can make contact with the brushes. During operation, this commutator will spin with the rotor and switch the polarity for each coil at the correct time, allowing for continuous motion. A major advantage of brushed DC motors compared to other motor types is that they do not require advanced electronics to be driven. If the motor is intended to rotate in one single direction, the motor needs to be connected only to a power supply. Alternatively, an H-bridge can facilitate bidirectional movement, which requires only four transistors to make. Since brushes are electronic contacts, lubricating them increases the contact resistance and can cause shorts. Therefore, this is not done, and the brushes will generate friction, causing them to wear over time. Eventually, they cease to make contact and need to be replaced, making brushed motors require periodic maintenance.

### Brushless DC motor

To eliminate the limitations of a brushed DC motor, brushless DC motors were designed. These DC motors, as the name suggests, have no brushes to mechanically switch the polarity of the coils. Instead, this is handled by a driver actively switching the polarity. Another difference is the placement of the permanent magnets and the coils. In a brushed motor, the coils were on the moving rotor and powered by the stationary brushes. Since the brushes are removed, the coils should now be stationary to allow them to be powered; otherwise, the wires connecting them would tangle after a few rotations. Therefore, the permanent magnets are placed on the stator. Most brushless DC motors have 3 phases, or windings, as well as a pole count for the permanent magnets. That is, the number of both north and south pole pairs on the rotor. To drive these motors, numerous methods with varying complexity exist, but every method uses three half-bridges to switch the phases between positive supply and ground. The simplest, called trapezoidal commutation, is most similar to the working of a brushed DC motor. Using the earlier-mentioned half-bridges, one phase will be connected to the positive supply, while another one is connected to ground. Since the phases are connected in either a Delta or Wye configuration, trapezoidal commutation allows for current to flow through two phases at a time, this time with electronics timing the flow instead of brushes. Since motors will never have an exact speed, this timing

can not be predicted, and hall sensors are integrated inside the motor to measure the rotor's magnetic field. Often, a BLDC motor has three of these sensors, spaced out 120° from each other. Since their purpose is only to time when the current should be inverted, and not to accurately determine the rotor's rotation, these are digital hall sensors, with a binary output, and a high output indicates that a magnetic south pole is close. Digital hall sensors are used to simplify control logic for a microcontroller and because they're cheaper to produce. Since the three sensors each output a single bit, a rotor state can be represented with 3 bits, and thus there are $2^3 = 8$ discrete states. The states 000 and 111 are, however, physically impossible to occur, leaving only 6 valid states. The states 000 and 111 represent situations where all three hall sensors simultaneously detect either the magnetic north or south pole. However, because the rotor has an even number of poles and the sensors are spaced evenly, it is geometrically impossible for all three sensors, separated by 120 degrees, to be aligned with the same pole type at the same time. Six discrete states give a positioning resolution of $\frac{360}{6} = 60°$, which is insufficient for accurate position control. When a motor has a pole pair count greater than 1, however, a state can represent multiple physical rotor positions, since there are multiple south poles for a high output. Therefore, a general formula for determining the positioning resolution for BLDC motors equipped with hall sensors is $\frac{60}{p}$, with p representing the pole pair count. Common values for the pole pairs lie between 2 and 4, leading to a positioning resolution between 15° and 30°, which is still insufficient for accurate positioning.

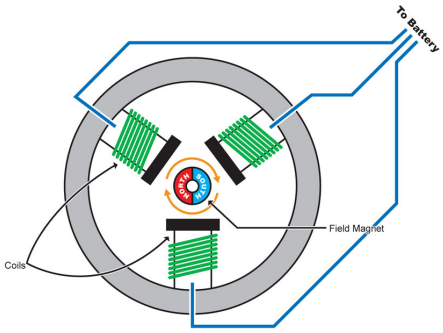


**(a)** Schematic showing the permanent magnets and coils inside a brushless DC motor
*Image taken from hpiracing.com [28]*

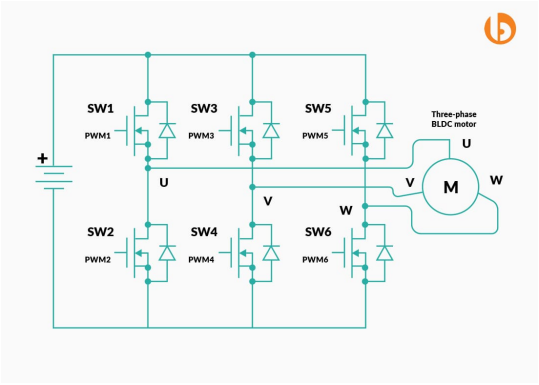


**(b)** Schematic showing the half bridges required for Trapezoidal Commutation
*Image taken from bacancysystems.com [29]*

### Encoders

To compensate for the poor, and for brushed motors even non-existent, positioning resolution of BLDC motors, encoders can be used to achieve closed-loop control. Many different types exist, but either an optical or magnetic one is most popular. An optical encoder is attached to the shaft of the motor and has a disk, moving with the shaft, that has a certain transparent pattern. On one side of the disk, is something emitting light, like an LED, and on the other side is a photosensor. The pulse train intercepted by this photosensor can then be related to the position and velocity of the shaft. A magnetic encoder requires a diametrically magnetized permanent magnet connected to the shaft and a Hall effect sensor placed close by. This hall effect sensor differs from the ones integrated in a BLDC motor because this one can output at a much greater resolution. Low-end encoders generally have a resolution of 8 bits, while high-end encoders can have resolutions up to 16 bits. Again, this leads to a positioning resolution of $\frac{360}{2^b}$, so $1.4°$ for low-end encoders, and $0.0055°$ for high-end encoders.

### Advanced control methods

The addition of an encoder allows for more advanced control methods to be used. Instead of the crude trapezoidal commutation, similar to the operation of a brushed motor, sinusoidal commutation or field-oriented control (FOC) can be used. Trapezoidal commutation assumes that when the current is switched between phases, it instantly changes from low to high. In practice, however, this is impossible and the time it takes for the current to rise induces a small ripple in torque. This ripple can cause vibrations at high speeds. Sinusoidal commutation works similarly to trapezoidal commutation, but feeds a sinusoidal current to the windings instead of a binary one. As long as every winding is 120°

out of phase, there will be no discontinuities in current flow, maintaining a constant torque curve. In practice, imperfections in both the fabrication quality of the motor and the control hardware will still induce a ripple, albeit much smaller compared to trapezoidal commutation. The most advanced control method is field-oriented control, or FOC.

### Stepper Motor

A stepper motor is a special type of brushless DC motor that rotates in discrete steps, often 200 steps per revolution. This is because of the unique design of the electromagnets in the stator. These electromagnets have small teeth, and when a gear-shaped rotor is used, the teeth of that rotor will align with the magnet's teeth when energized. The magnets are then placed in a way so that when magnet A is energized, and thus the teeth of the rotor are aligned with magnet A, the rotor's teeth are slightly offset from magnet B. Then, when magnet A is turned off, magnet B is turned on, and the rotor aligns with that magnet. This causes a small rotational movement and is called a step. The total number of steps is determined by the number of teeth in the rotor and the number of magnets placed in the stator. The animation below shows a simplified, rotating mechanism. *Animations only work in Acrobat Reader; the individual frames are placed in the appendix if you are unable to view the animation.*

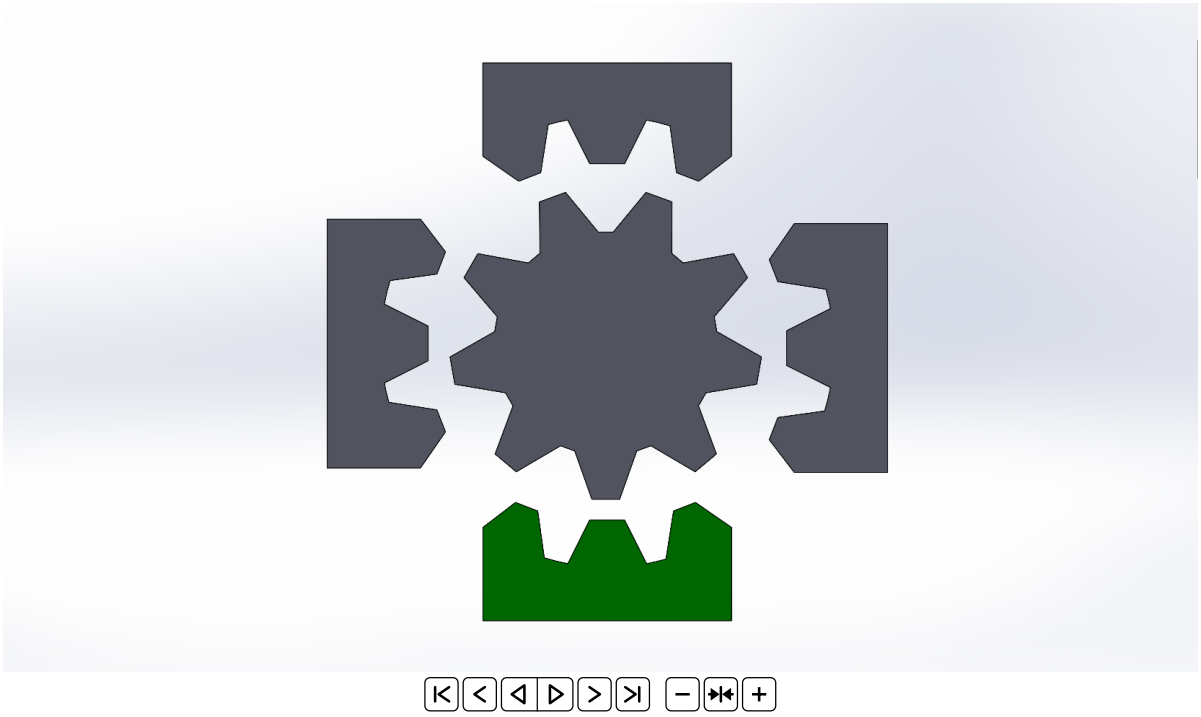

**Figure 4.7:** Simplified mechanism showing the operation of a stepper motor. *[Animation made in SolidWorks]*

The discrete nature of stepper motors allows for accurate position control without an encoder. With a lack of feedback, this will be open-loop control, so when, for example, a large load is applied for which the motor is unable to provide enough torque, the controller still thinks the shaft is rotating, while in reality it is stationary, and the position will be lost. This is called step loss. As long as there is no excessive step loss, however, they offer cheap position control and are therefore often used in 3D printers or CNC machines.

As mentioned, most commonly available stepper motors make 200 steps per revolution, which leads to a step angle (the number of degrees that the shaft will turn per step) of 1.8°, comparable to the accuracy of a regular BLDC motor with a low-end encoder. This can, however, be reduced by microstepping. Microstepping adjusts the current fed to the electromagnets, allowing a magnet to be turned on with only a fraction of the usual power. When properly controlled, this means that the motor will have multiple intermediate steps, also called microsteps. Many different drivers that can microstep exist, with resolutions ranging from 2 microsteps (that is, only 1 intermediate step) to 1024 microsteps and even more. Take a driver with a resolution of 16 microsteps, and a stepper motor with 200 steps per

revolution. This driver can then increase the steps per revolution to $16 \cdot 200 = 3200$ microsteps per revolution, making rotation much smoother and precise. Microstepping also has disadvantages, and the biggest one is a reduction in incremental torque. Incremental torque is the torque the motor can deliver when moving from one step to the next, and follows the following formula when microstepped is used.

$$T_{inc} = T_{HFS} \cdot \sin \frac{90}{N_{microsteps}} \tag{4.1}$$

Where $T_{HFS}$ is the holding torque for a full step.

Putting some common numbers of microsteps in a table gives

| Microsteps | Percentage of torque |
|---|---|
| 1 | 100% |
| 2 | 70.71% |
| 4 | 38.27% |
| 8 | 19.51% |
| 16 | 9.80% |
| 32 | 4.91% |
| 64 | 2.45% |
| 128 | 1.23% |
| 256 | 0.61% |

**Table 4.2:** Percentage of incremental torque for some common numbers of microsteps

From this table, it can be approximated that every time you double the number of microsteps, you halve the amount of incremental torque the motor can provide. This reduction in incremental torque can lead to scenarios where the driver receives a pulse to move 1 microstep, but the motor can not provide the torque required to make this movement. Luckily, this does not lead to step loss, as the torque builds up with each successive microstep, ultimately allowing the motor to move to the latest microstep position. It does, however, diminish the positive effects of microstepping, since the expected microsteps are not taken.

## 4.2. Chosen actuator

As mentioned in Section 4.1.1 - Design Choices, for the mechanical system, a rack-and-pinion setup was chosen. This requires a motor to drive the pinion, for which a stepper motor was chosen. Stepper motors provide good precision for a reasonable price and keep the electrical system simple. Both brushed and brushless motors equipped with a high-end encoder would theoretically have better precision and performance. This project requires very slow movement, however, which would require the more advanced sinusoidal commutation, or even FOC. Making a driver capable of these control schemes would be a project on its own, and buying a commercially available one falls out of the budget. Therefore, a compromise was made on precision, and a NEMA17 stepper motor was selected.

## 4.3. Required components

As mentioned in Section 4.1.2, stepper motors initially have a positioning accuracy of only 1.8°. Using microstepping, this can be decreased substantially. This does require a driver capable of microstepping, for which the A4988 was selected. The A4988 is one of the cheapest and simplest drivers available and lacks many features that slightly more expensive drivers have. These features include, but are not exclusive to, stall detection, better cooling, and silent operation, which are all irrelevant for this implementation. The motor used will only take a (micro)step ever so often, and not do fast, continuous

motion, where these features would be a great addition. Control is also made easy by providing a simple STEP / DIR interface. This consists of two pins, a STEP pin and a DIR pin. When the STEP pin receives a pulse, it will take a step in the direction specified by the DIR pin. Additionally, the A4988 allows microstepping up to 1/16, which was deemed enough for a proof-of-concept. The driver also needs to be controlled by a microcontroller, such as an Arduino or an ESP32. Finally, the motor needs power. For this, a DC power supply capable of providing a voltage between 12V and 24V is required. The Meanwell RD-50A provides both a 12V and a 5V DC output, allowing both the microcontroller, which needs 5V, and the motor to be powered by a single power supply without the need for any voltage converters.

The following table will list the components chosen.

| Component type | Component chosen |
|---|---|
| Motor | NEMA17 Stepper Motor |
| Driver | A4988 |
| Microcontroller | ESP32 |
| Power supply | Meanwell RD-50A |

**Table 4.3:** Chosen components

## 4.4. Resolution analysis

This section will analyse the resolution achieved with the design choices made earlier in this chapter. First, the step angle of the stepper motor needs to be determined. Since the A4988 driver, capable of microstepping up to 1/16, is used, the step angle equals $1.8°$, the full step angle, divided by 16, the amount of microsteps, giving a step angle of $0.1125°$. To equate this step angle to a linear step distance of the rack-and-pinion mechanism, we need the gear's pitch circle. This is an imaginary circle that would be tangent to the pitch circle of a mating gear. Mating gears overlap slightly, so this pitch circle is slightly smaller than a circle made by tracing the tips of the gear's teeth.

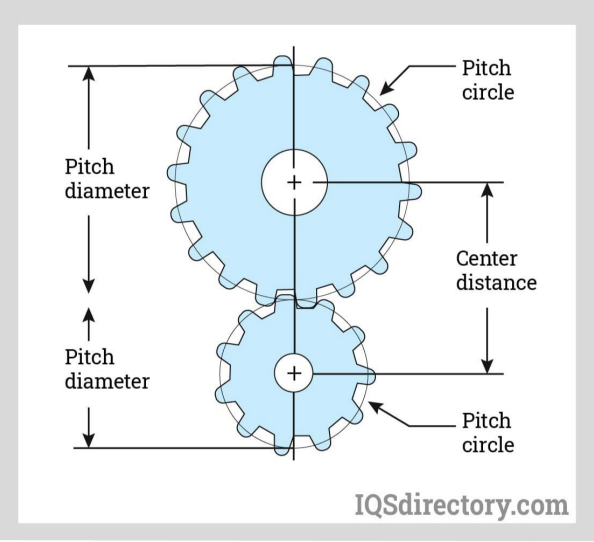


**Figure 4.8:** Schematic showing the pitch circles for two gears
*Image taken from iqsdirectory.com [30]*

The linear distance travelled by the rack per revolution is then equal to the circumference of this circle. The gear used in the prototype was designed in SolidWorks, using SOLIDWORKS Toolbox. This gives you the option to specify the module and the number of teeth, along with some other variables irrelevant

to this analysis. Module is a value relating the pitch diameter to the number of teeth, by

$$M = \frac{P_D}{N_{teeth}} \ [m] \tag{4.2}$$

The gear used in the prototype has a module of $0.8mm$, with $32$ teeth. This gives a pitch diameter of $0.8 \cdot 32 = 25.6mm$. Therefore, the distance travelled by the rack can be calculated as

$$D = \pi \cdot P_D \cdot \frac{\theta_\Delta}{360} \tag{4.3}$$

Where D is the distance travelled, $P_D$ is the pitch diameter and $\theta_\Delta$ is the angular displacement of the gear in degrees. Setting $\theta_\Delta$ equal to the stepper motor's step angle calculated earlier, gives a step distance (the distance travelled by the rack per step) of $D = \pi \times 25.6 \times \frac{0.1125}{360} = 0.0251mm = 25.1\mu m$.

## 4.5. Motor casing

Since the actuator will be inside an incubator, with high humidity, the motor will need to be protected for corrosion. For this, a casing was designed that could act as the guide rail for the rack at the same time. The casing is a simple hollow box, slightly bigger than the motor itself, in which the shape of the motor is carved out. To be able to replace the motor, this casing consists of a base and a lid, and is split at the height of the motor's shaft. As mentioned before, the base has a guide rail that sticks out slightly. Additionally, the lid has a small hole for the wires to stick out. To fill up the inevitable free space left between the base and the lid when they're placed on top of each other, a gasket should be used. Finally, once the motor is placed inside the casing, the hole with wires should be filled up with a seal like the one explained in Section 5.1.3. For rapid prototyping, a FDM-printer with PLA filament was used to print this casing. PLA is cheap (€10 for 1kg) and prints fast with a FDM-printer, but it is not humidity proof and therefore not a suitable material for this casing. There are methods to coat PLA with a hydrophobic film [31], but this is a temporary solution since the coating will degrade fast inside the high-temperature incubator. For this proof-of-concept, it was chosen to keep the casing made from PLA, but for future implementations that will go inside the incubator, it is recommended to print the casing from different materials, such as ASA which offers superior heat and humidity stability [32].

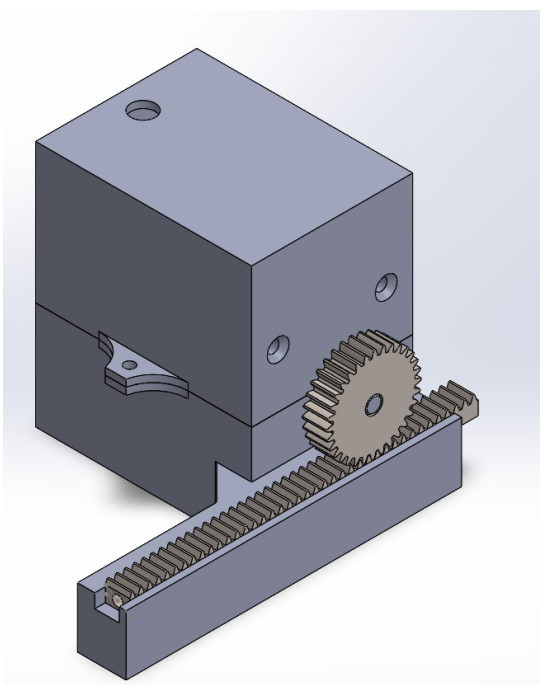

**(a)** Motor casing with rack and pinion mechanism.

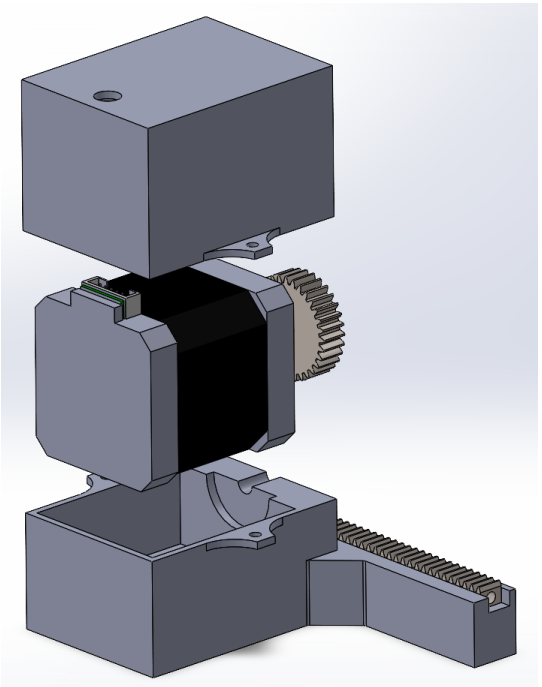

**(b)** Exploded view for the motor casing.

# 5

# Design of the well

This chapter will describe the design process of the well and its subsystems. The design decisions are based on the program of requirements, as listed in chapter 2, as well as the solutions discussed in section 3.2. For this part of the design process, two potential options were created, after which one was chosen to be built as a prototype, as briefly discussed in Section 3.2. Some 3D designs for the alternate option can be found in Appendix B. This chapter will first describe the general design aspects that are necessary to build a working well and provide actuation to one of the support pillars, after which the specific design aspects to solve the sensing issues are given. Unless stated otherwise, all parts are printed using Formlabs Biomed Clear resin to comply with the requirement for biocompatible materials inside the well environment.

## 5.1. General design decisions

### 5.1.1. Pillar design and connecting to the actuator

The first concern in the design of the well is providing a connection between the actuator described in Chapter 4 and one of the support pillars of the muscle bundle within the well. To achieve this, one of the pillars inside the well needs to be connected to the actuator via a rod- or beam-like support structure. In order to achieve this, the pillar has been designed to enter horizontally from outside to well through the use of a $3mm$ diameter cylinder, which can be connected to the actuator. Inside of the well, the cylinder shape of the pillar will shrink to $0.8mm$ in diameter and bend downwards into the chamber. At the end of the pillar is a cap of $1.5mm$ in diameter, to ensure the muscle bundle can attach itself firmly. This cap is positioned $0.5mm$ above the floor of the well. No part of the pillar is made from elastomeric material, to ensure the muscle cannot flex during the growth phase. This approach avoids the need for more complex locking or measuring subsystems as discussed in Section 3.2. The corresponding 3D model of the pillar is shown in figure 5.1.

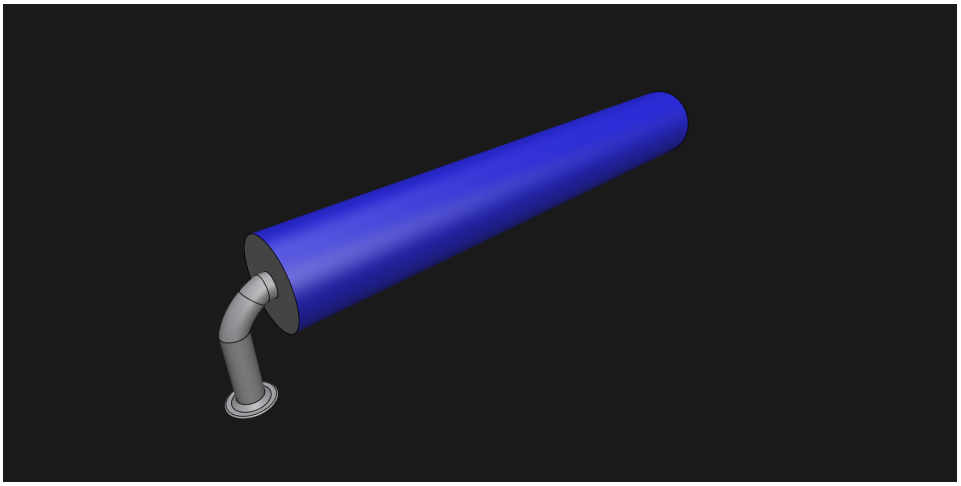

**Figure 5.1:** 3D design of the actuated pillar

### 5.1.2. Well shape and chamber

Conventional well designs typically incorporate a round enclosure, mirroring the shape of a standard Petri dish [1, 5, 10]. However, because the current design requires a connection to an actuator outside the well, a round shape is undesirable. Consequently, a rounded square shape was adopted to facilitate a straight-walled exit point for the actuated pillar to exit. This exit point is marked by a hole inside the well wall, made $3.2mm$ in diameter, which minimizes friction-related performance issues. The interior of the well houses a chamber that accommodates the muscle support pillars. The actuated pillar, as previously described, rests within a small indent in the chamber that enables free linear motion. A side overview of the well and its chamber can be seen in Figure 5.2. A few measurements as seen from the top of the well can be seen in Figure 5.3.

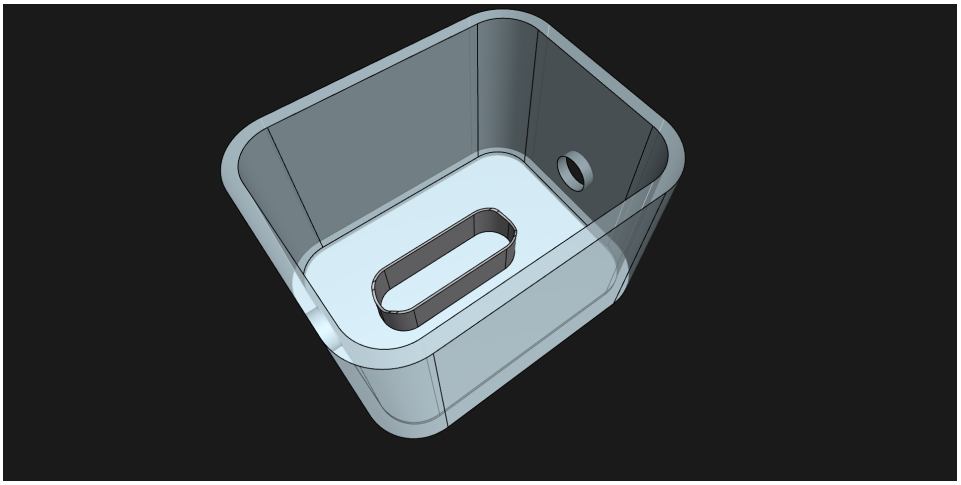

**Figure 5.2:** The design of the well as seen from the side

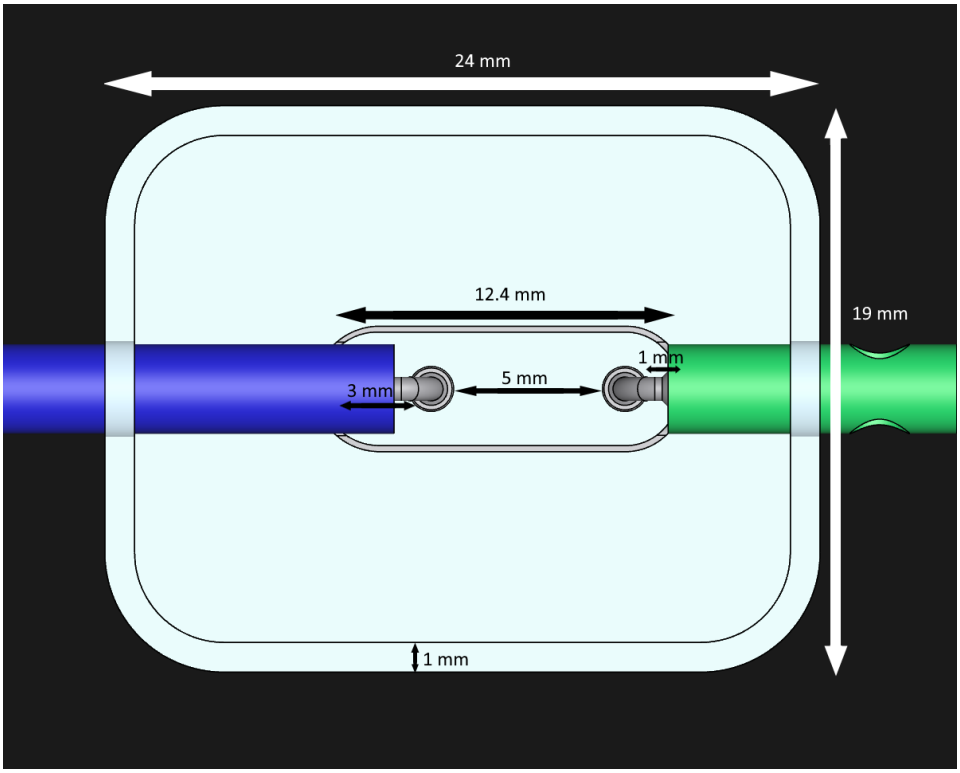


**Figure 5.3:** An overview of some important measurements of the well.

### 5.1.3. Sealing

To seal the previously mentioned opening in the well, a small hollow cone, fabricated via 3D printing with Formlabs Elastic 50A resin is employed. The cone is $3mm$ tall and ranges from a $3mm$ wide diameter at the top to an approximately $6mm$ wide diameter at the bottom. The cone is secured to both the actuated pillar and the well wall such that it remains highly flexible while offering minimal resistance. Although an O-ring could have provided equivalent sealing, it was not selected for this design because its use would have introduced additional resistance during the sliding motion of the actuated pillar. A 3D design of the seal can be seen in Figure 5.4.

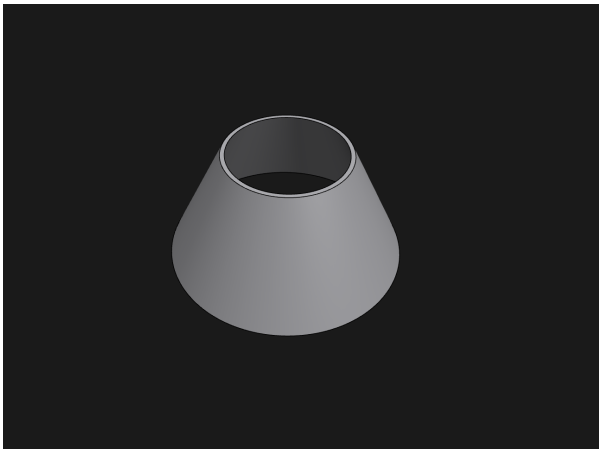

**Figure 5.4:** 3D design of the seal

### 5.1.4. Lid

To isolate the well from external influences, a lid was designed to cover the well. The interior of the lid features two small spacers placed at each corner. In conjunction with the lid's dimensions (which

exceed that of the well by $0.4mm$), this arrangement permits the required gas exchange. The lid also houses 4 holes of $0.5mm$ in diameter, to accommodate the carbon electrode rods for the electrical stimulation of the muscle. These electrodes are positioned on each side of both pillars, adjacent to the chamber and aligned parallel to the muscle bundle. The electrodes and their subsystem will be further explained in Chapter 6.

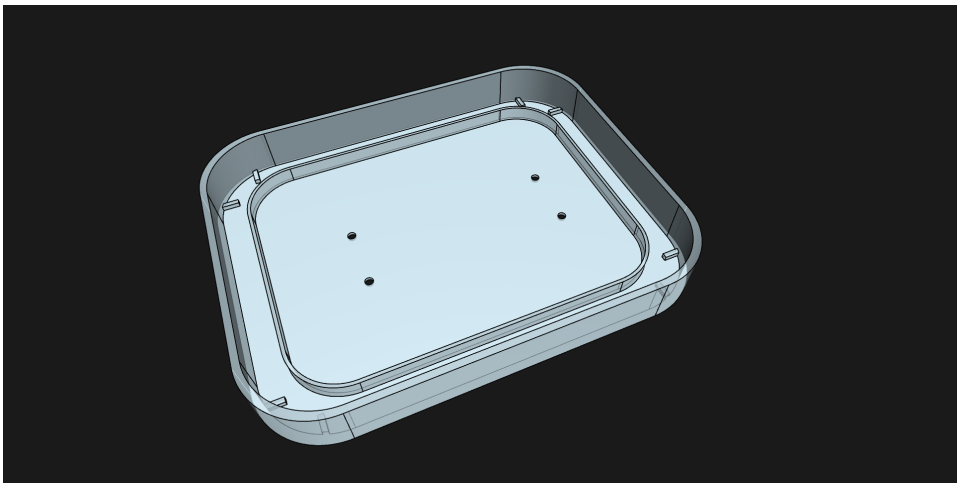

**Figure 5.5:** 3D design of the lid

## 5.2. Solving the flexible pillar dilemma

To address the problem outlined in Section 3.2, a design was developed based on the first proposed solution. In this configuration, both pillars were fabricated using Formlabs Biomed Clear resin, which exhibits minimal bending from the muscle bundle. The design approach involved creating the non-actuated pillar as a mirrored replica of the actuated pillar, extending out of the well in the direction opposite to the actuated one. This configuration is illustrated in Fig. 5.6a. In order to facilitate this, the well contains another opening which is sealed in the same way as described in Section 5.1.3.

A custom-designed basket was integrated into the well structure to maintain the vertical alignment of the non-actuated pillar. The basket featured upright extensions on both sides, incorporating a 2 mm diameter hole spanning laterally between them. The pillar was designed with a corresponding cutout, and can sit securely within the basket. During the muscle growth phase, a matching pin can be inserted into the cutouts, which fixes the pillar to a locked position. After the growth phase, if the user wishes to measure the contraction of the muscle bundle, the pin can be removed, allowing the pillar to slide when the muscle pulls and subsequently releases it.

The entire assembly, including the well and basket, was mounted onto a support plate, which also served to attach the system to the actuator. Approximately $2mm$ from the end of the pillar, a secondary support structure was positioned such that its top aligned with the centre of the pillar. A polydimethylsiloxane (PDMS) segment was placed between the pillar and this support structure. This PDMS bends when the muscle bundle pulls on the pillar during stimulation, and also pulls the pillar back when the muscle stops contracting. The bending of this PDMS can be measured optically, to determine the force of the muscle contraction. Figures 5.6b and 5.6c present viewpoints of the basket, the support structures, and their integration with the pillar and pin mechanism.

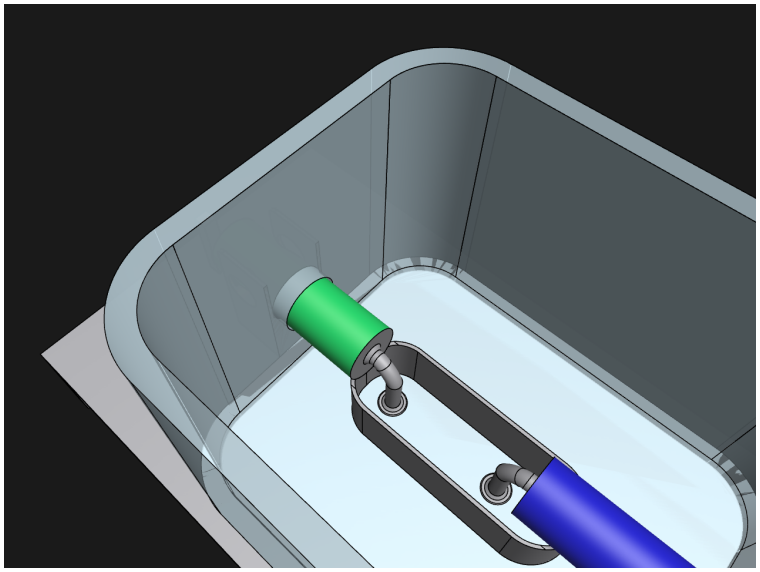

**(a)** A view of the design inside the well.

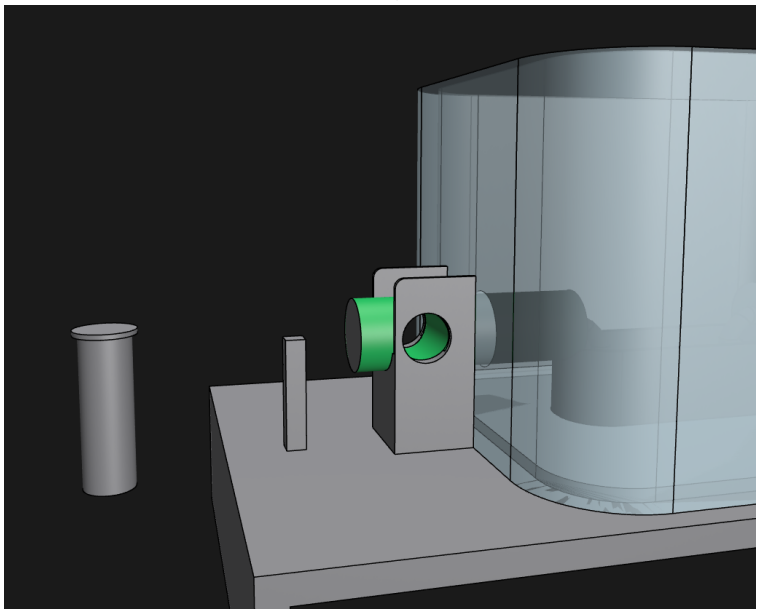

**(b)** A view of the design outside the well.

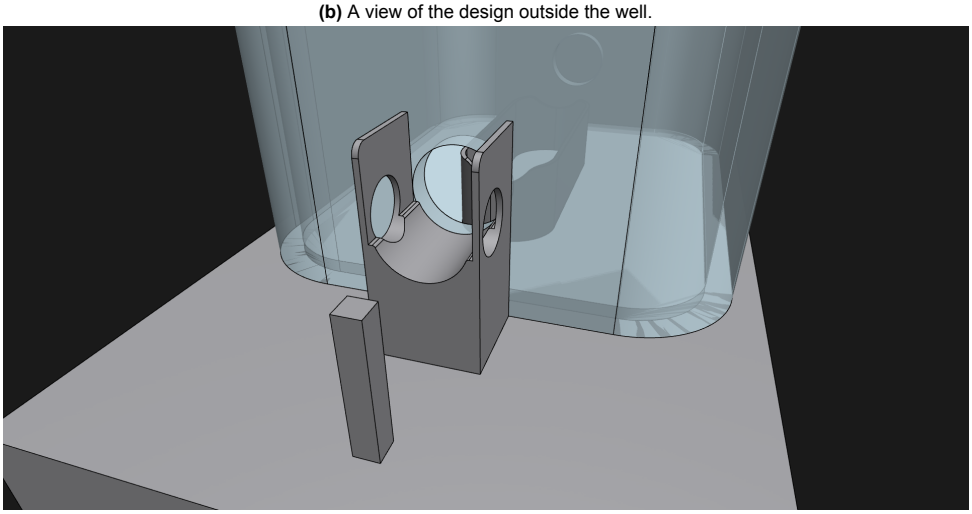

**(c)** A view of the basket holding the sliding pillar.

**Figure 5.6:** Different viewpoints of the design.

# 6

# Electrical subsystem

As stated in the Program of requirements (Chapter 2), the muscle should be electrically excitable. In previous studies, this was often done using electrodes inserted near the muscle bundle, which would provide necessary muscle stimulation. This chapter focuses on the design of the electrodes regarding placement, material selection, and electrical signal type and generation.

## 6.1. Electrodes

### 6.1.1. Materials and placement

As already discussed in section 3.3, carbon electrodes were selected due to their compatibility and low cost. Also, ease of manufacturing or acquiring the electrodes was a factor in making the final selection. Due to the design geometry, it was not possible to place the electrodes exactly behind the muscle bundle. Therefore, the choice was made to use four electrodes, one pair of two on each side of the bundle placed closely together on either side of the sliding rods. In this way, the electric field remains in the direction of the muscle bundle. The carbon rods are cut to 4 pieces of $18mm$, with their solder joints protruding outside of the well lid when positioned at the same height as the caps of the support pillars. Since the solder joints are not in direct contact with the cells and medium inside the well and therefore toxicity would not be an issue (see section 1.1), the decision was made to use lead-tin as solder.

## 6.2. Function generation and amplification

In previous studies, a number of different signal types, frequencies, and amplitudes were used. These include the following types of signals:

| Signal type | Frequency | Amplitude | Study |
|---|---|---|---|
| - | 2 Hz | - | [1] |
| Square wave | 0.5, 20 Hz | 5V | [3] |
| Biphasic rectangular pulse | 0.5-3 Hz | - | [5] |
| - | 20-75 Hz | 2-5 V | [7] |
| Biphasic signal | 1 Hz | - | [20] |

**Table 6.1:** Different electrical signals used for muscle stimulation

In addition, the duration for which this signal was applied, was around 5-10 ms [7] [20].

For this design, the goal was to stimulate the muscle with a square wave of variable frequency and an amplitude of 0-5 Volts. This was achieved using the microcontroller's built-in PWM functionality, through which a rectangular signal of given frequency and duty cycle can be specified. The amplitude level can then be controlled using an op-amp [33].

# 7

# Assembly and results

This chapter will describe the process of implementing the previously designed parts, as well as assembling the full prototype. At the end of this chapter, the main results from this prototype will be discussed. This chapter will not discuss parts of the design that can only be tested with live muscle cells, as this would not fit within the time constraints of the project. This mainly concerns the non-actuated pillar within the well. As such the results will limit themselves to the actuation and signal generation.

## 7.1. UI

To make interacting with the system easy, a user interface was developed. This user interface is displayed on a 4-inch TFT LCD display, with a resolution of 320 by 480 pixels and touchscreen support. The display is integrated in a casing that will be placed outside the incubator, additionally containing the power supply, microcontroller, signal generator, and motor driver.

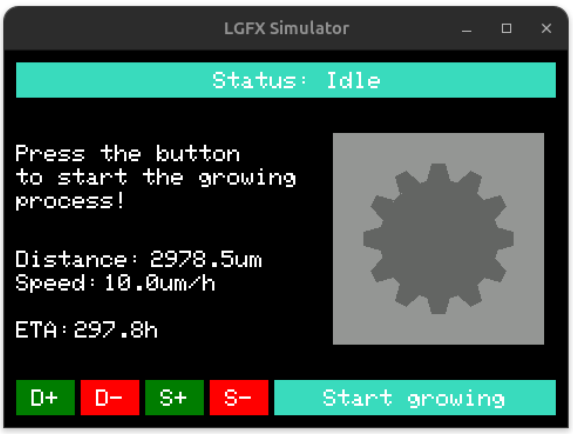


**Figure 7.1:** UI in its idle state

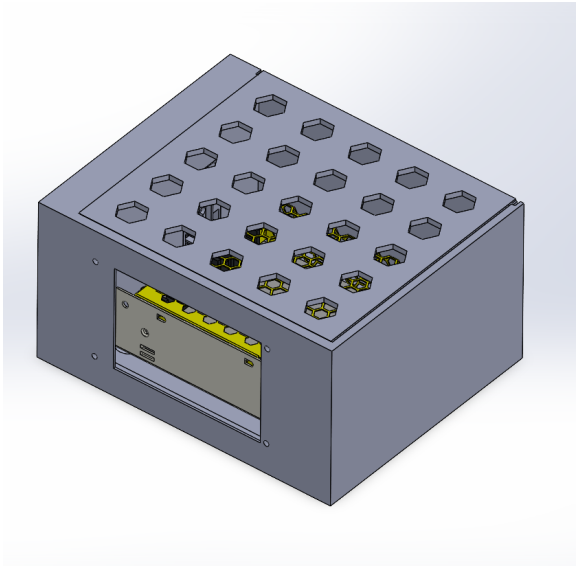

**Figure 7.2:** The casing outside of the incubator for the power supply and screen. The lid can be slid off.

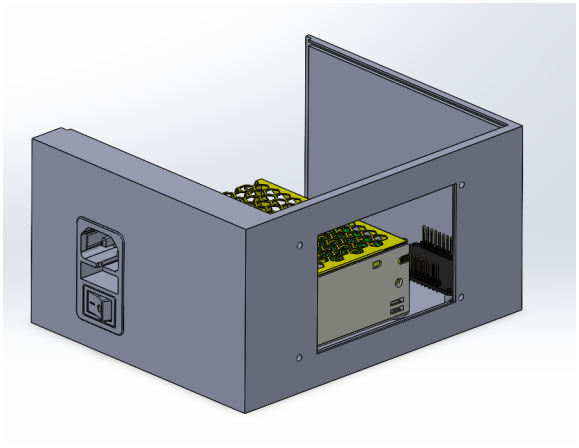

**Figure 7.3:** The casing outside of the incubator for the power supply and screen without a lid, showing the power connector.

Interfacing with the display is done with the SPI protocol through the microcontroller. To assist in the low-level communication and control of the display, numerous libraries exist that provide high-level functions for ease of use. For this project, it was chosen to use LovyanGFX (LGFX). This library has advanced sprite support, making the display look smooth during relatively high refresh rate animations. When sprites are not used, the display's driver (ILI9488) sends pixel information while they are computed. TFT displays, however, refresh slowly. If the screen is not cleared before a new image is displayed, this can cause tearing, where parts of the old image and the new image are visible at the same time. Nevertheless, clearing the screen before drawing a new image does not give smooth animations either, because the screen might appear to flicker, as only parts of the image are displayed while other parts are still black. Using sprites, their pixel information is first stored in the display's internal RAM and only sent once as a complete image, fully eliminating tearing and flicker. Figure 7.1 shows the UI in its idle state. The top bar, showing the current status, is present in every state, while the contents and the bottom button, or bar, change with state. The image on the right side is a simplified version of the actuator. Even though LGFX provides easier-to-use functions than the low-level communication the display expects, it still requires the creator to draw everything using a few primitive shapes, like rectangles, triangles, and circles. Alternatively, it is possible to make images on a PC and convert them to raw C arrays which will be stored on the microcontrollers internal memory. This, however, gives limited control for animations. Additionally, the microcontroller's memory is limited to only 4 MB. Therefore, it was chosen to use the primitive shapes and keep the UI simple. When the user presses the "Start growing" button, the growing process will start. The UI allows the user to specify, in micrometers, how far the actuator should extend, and at what speed. Finally, the ETA will inform the user about the time this process will take.

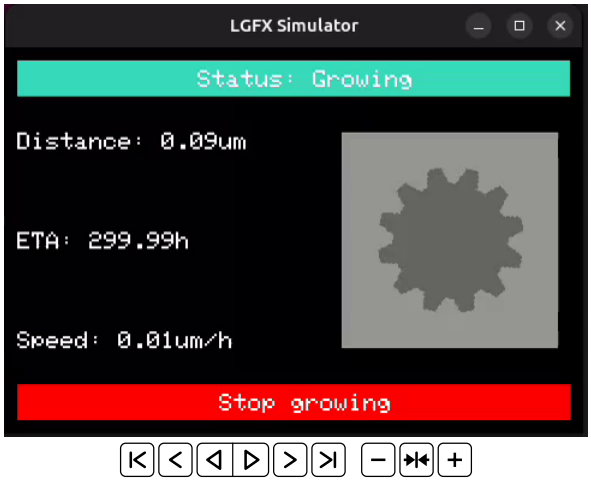


**Figure 7.4:** UI during the growing phase. *[Recorded using LGFX-simulator-SDL]*

During the growing process, the UI will show some limited statistics to monitor the progress, as can be seen in the animation above. *Again, animations are only visible in Acrobat Reader.*

After the growing phase is completed, the UI will allow the user to specify a wave type and frequency to stimulate the muscle.

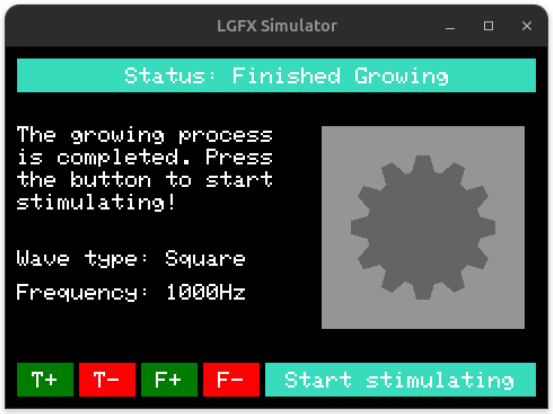


**Figure 7.5:** UI after the growing phase is completed

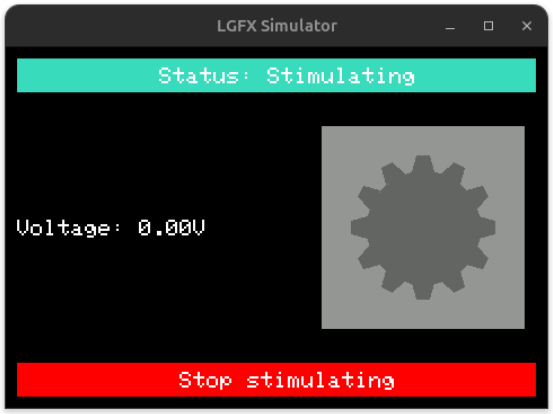


**Figure 7.6:** UI during the stimulating phase

The final state the UI could be in, is the stimulating phase. It was preferred to show the active waveform on the screen, along with some extra statistics, but this was difficult to implement with LGFX. Therefore, it was chosen to drop the waveform and only show the current amplitude as statistic, because the UI is not a priority for this project. By pressing the ”Stop stimulating” button, the UI will return to the ”Finished Growing” status. To reset the device and start growing again, the power can be turned on and off.

## 7.2. Printing and assembly

### 7.2.1. Printing the well

The design of the well was printed using a Formlabs 4B Medical 3D printer, the result of which can be seen in Figure 7.7. The two cylinders protruding out of the base are used to secure the printed well to the actuator. During printing, the support structure intended to hold the PDMS for contraction force measurement was detached. As has been explained, this did not concern the test results reported in this chapter. The holes inside the lid were also misprinted, but since no medium or muscle cells were inside the well, the electrodes did not have to be physically inside the well to test their results.

**Figure 7.7:** The well after 3D printing.

### 7.2.2. Connecting the well and actuator

The well and actuator are connected via the previously explained cylinders protruding out of the well and matching entry points inside the actuator casing. The actuated pillar is connected via another entry point inside the rack. The result of this can be viewed in Figure 7.8. As can be seen in the figure, the well is slightly slanted compared to the actuator, due to slight misalignments in the entry points, but for testing the actuation of the support pillar, this does not present any problems. Additionally, the hole for the actuator shaft has too low of a tolerance, giving excess friction in this print.

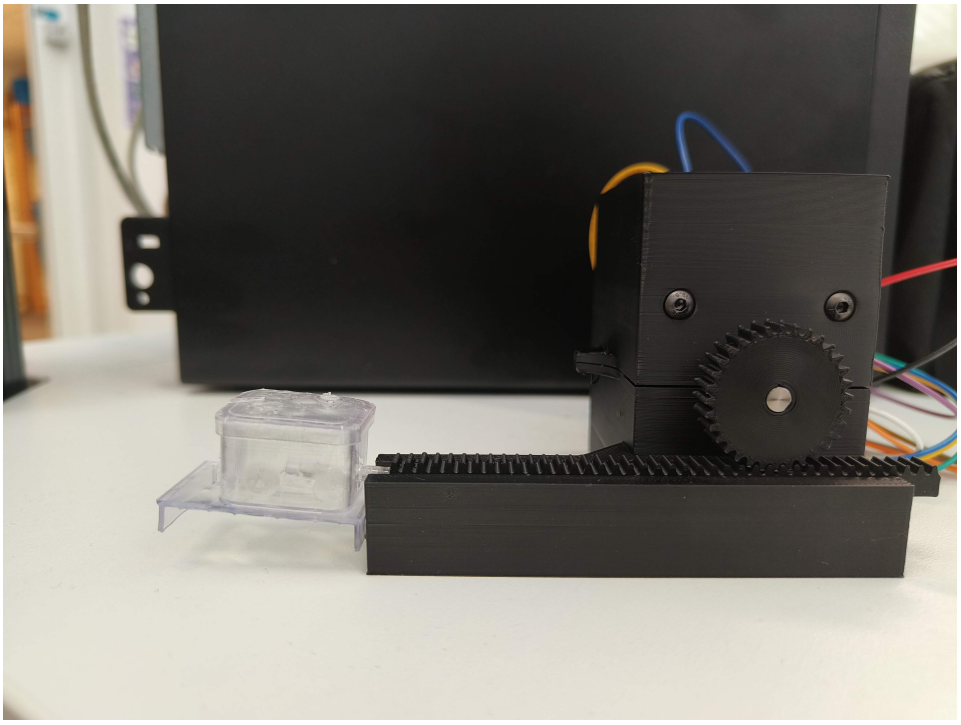

**Figure 7.8:** The well and actuator setup after connecting the two.

## 7.3. Results

### 7.3.1. Actuation results

After assembling the prototype, visual measurements were done using a microscope available in the Tellegen hall in EWI. This proved that the actuator behaves as expected, taking discrete steps. Due to time constraints and the unavailability of calibrated measuring instruments at the time of testing, an estimated measurement was used by recording a video and comparing pixel distances between frames, to verify the resolution analysed in Section 4.4. Due to high friction in this unlubricated rack's guide rail, and in the hole for the shaft, as mentioned in Sections 4.1.1 and 7.2.2, it was chosen to move with 2 microsteps at a time for this test, because 1 microstep could not provide enough torque to move the gear. Section 4.1.2 explains why this happens. The video was recorded by holding a phone in front of one of the microscope's lenses, which leads to some small jitter in the video, but was deemed acceptable to estimate the step size. Every frame had a small, 4-pixel-high dark blue rectangle on top of the cap, which was used as a reference line to determine the displacement.

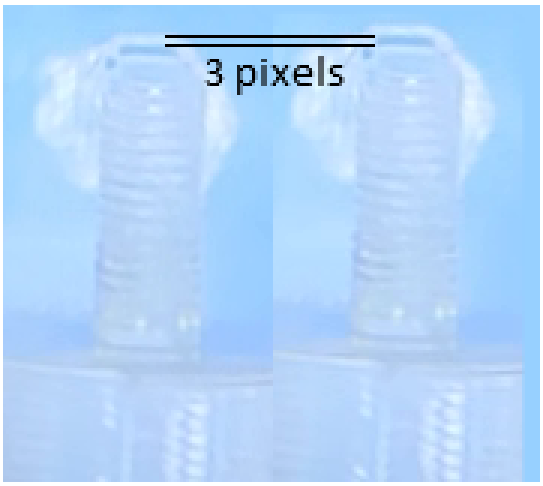


**(a)** Measurement after step 1

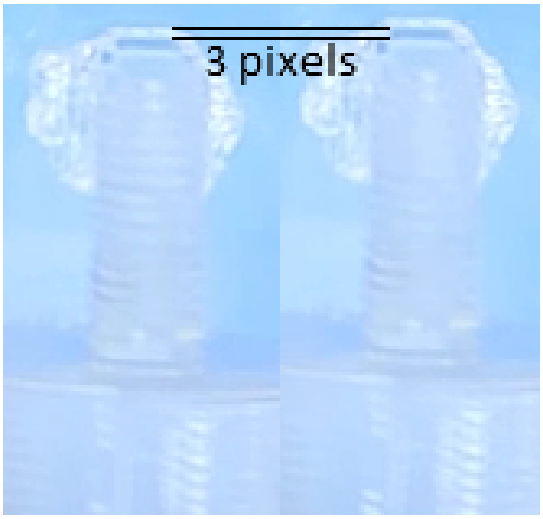


**(b)** Measurement after step 2

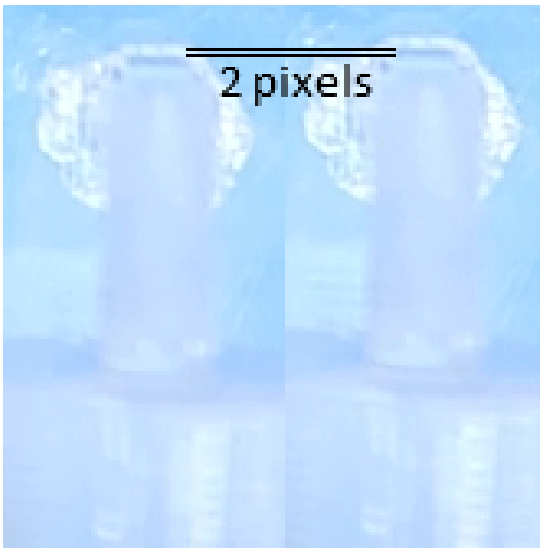


**(c)** Measurement after step 3

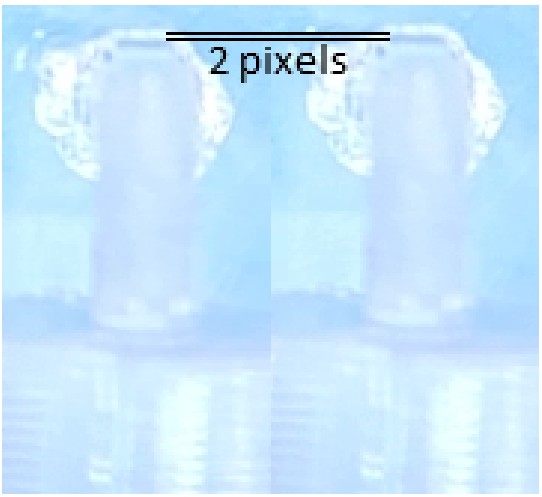


**(d)** Measurement after step 4

**Figure 7.9:** Four measurements for the step size

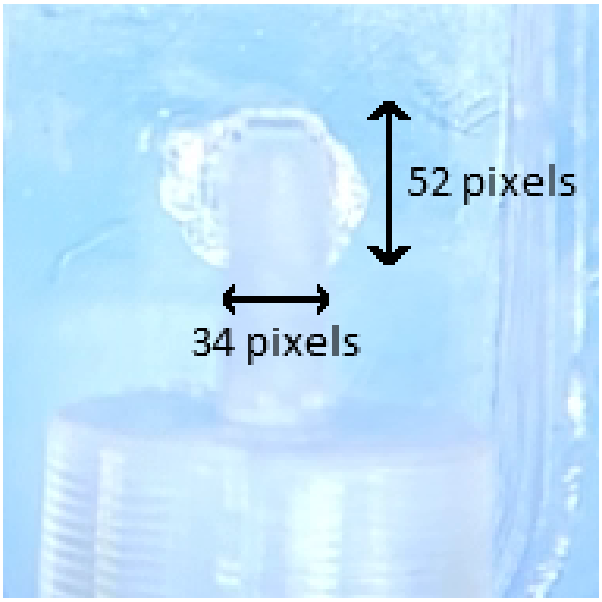


**Figure 7.10:** Reference pixel distance

Using the reference visible above, the diameter of the cap is measured to be 52 pixels and is designed to be 1.5mm, and the pillar's diameter is measured to be 34 pixels and is designed to be 1mm. Therefore, one pixel equals about $\frac{1}{2}(\frac{1.5 \cdot 10^{-3}}{52} + \frac{1 \cdot 10^{-3}}{34}) = 29.1 \cdot 10^{-6}\, m = 29.1 \mu m$. Taking the average of the four measurements leads to a step size of 2.5 pixels, or $72.8 \mu m$. This is, however, as mentioned before, the step size of 2 microsteps, so the actual achievable step size with this driver and setup is $36.4 \mu m$ with proper lubrication or a higher torque motor. The values calculated here are, of course, estimations, and actual values will deviate from these estimations, due to a low resolution and possible motion blur, combined with the fact that the video was not recorded exactly above the actuator shaft.

The full video can be found on YouTube [34].

### 7.3.2. Electrical results

The method used for the generation of signals, as described in 6.2, yielded some results, as can be seen in 7.11. This figure shows two waveforms, one an amplified version of the other.

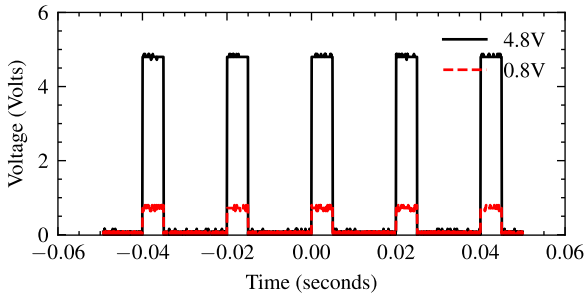


**Figure 7.11:** Example waveforms of a 25% duty cycle, 50 Hz signal

The resistance of the carbon electrodes used for this project was measured to be around $100\Omega$. Using two electrodes in parallel on both sides of the muscle bundle, the total resistance of the system should be at least $100\Omega$. It should be noted that although this has not yet been tested, when using the 5V output of the power supply [35], the given voltage levels could be supplied to the muscle, since the maximum supply current of the power supply is far above the current required.

# 8

# Discussion and Conclusion

This thesis has provided a muscle on a chip design focused on displacing the support pillars, made possible with the combination of mechanical, electrical, and biomedical research. During the 3D printing process of the well, some small pieces broke off, such as the support structure onto which the piece of PDMS for use in optical measurements would have been placed. It would thus be recommended that the design be updated to try and avoid these issues, although parts breaking is an unavoidable issue when it comes to 3D printing. The lid also proved to be difficult for the printer to fabricate. A thicker lid design is recommended to ensure improved handling during the printing process. Although these issues did not greatly affect the current prototype testing, since live muscle cell experiments were beyond the scope and time constraints of this project, they nevertheless highlight areas for refinement.

The actuator provided the results necessary as stated in the programme of requirements, although the openings for the pillars should be made slightly larger, as they currently are too precise and narrow and provide friction when the pillars are not perfectly aligned. In future test cases, it would be recommended to have the carbon electrodes soldered by a specialized professional or company, as the current solder joints are imprecise and can provide a bad or inconsistent electrical connection after some time exposed to the incubator environment. To conclude, the main goal of the project, being the displacement of the support pillars, is achieved and provides satisfactory results, and as such offers a promising foundation for any future works that aim to implement the same premise.

## 8.1. Future work

- The design should be tested with live muscle tissue. This mostly concerns the lockable pillar and its corresponding flexible bit. Additionally, the electrodes should be tested inside the medium.
- The 3D design of the well should be adjusted to better accommodate the inaccuracies of a 3D printer, as well as to provide better sliding properties to the support pillars.
- The design could be altered or provide a base to a future design, which focuses on scaling the project to multiple wells. Other improvements include a different, more accurate measurement setup, such as the use of strain gauges or Hall sensing.
- While the current actuator is accurate enough to fulfil the requirements, more strides could be made in this department if desirable. This could be done with the help of gearboxes or higher-level microstepper drivers. For even better precision, at a higher cost, piezoelectric actuators could be explored further.
- The amplification of the electrical signal could be made digitally controllable, allowing for more ease of use and greater accuracy. In addition, if needed, the capacity for generating different waveforms other than rectangular waves could be added.
- The mechanical system is currently 3D-printed. This is fine for prototyping and proving the concept works, but a proper system should be made out of a better material, such as stainless steel, which can also be lubricated to reduce friction.

# A

# Individual animation frames

Since this document contains two animations only visible in Acrobat Reader, this appendix chapter will show the individual frames for readers unable to view the animation.

## A.1. Stepper Motor

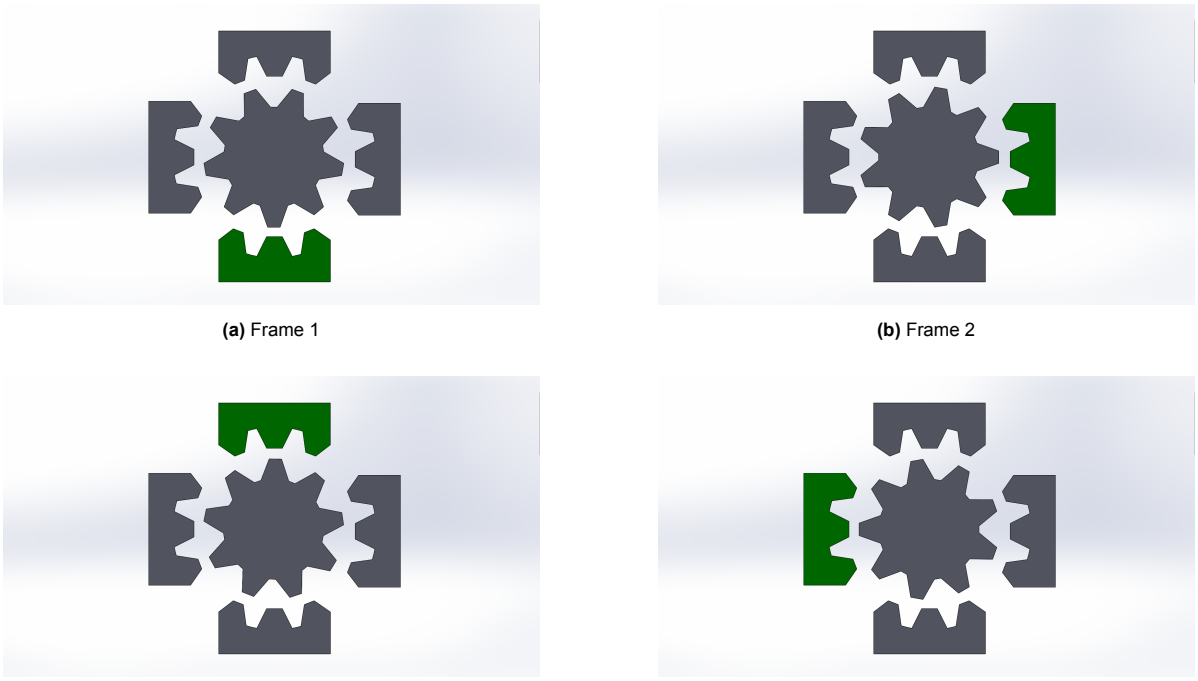

**(a)** Frame 1

**(b)** Frame 2

**(c)** Frame 3

**(d)** Frame 4

**Figure A.1:** Individual frames for the stepper motor animation.

## A.2. UI

Since this animation contains 450 frames, only a few snapshots are included in this appendix.

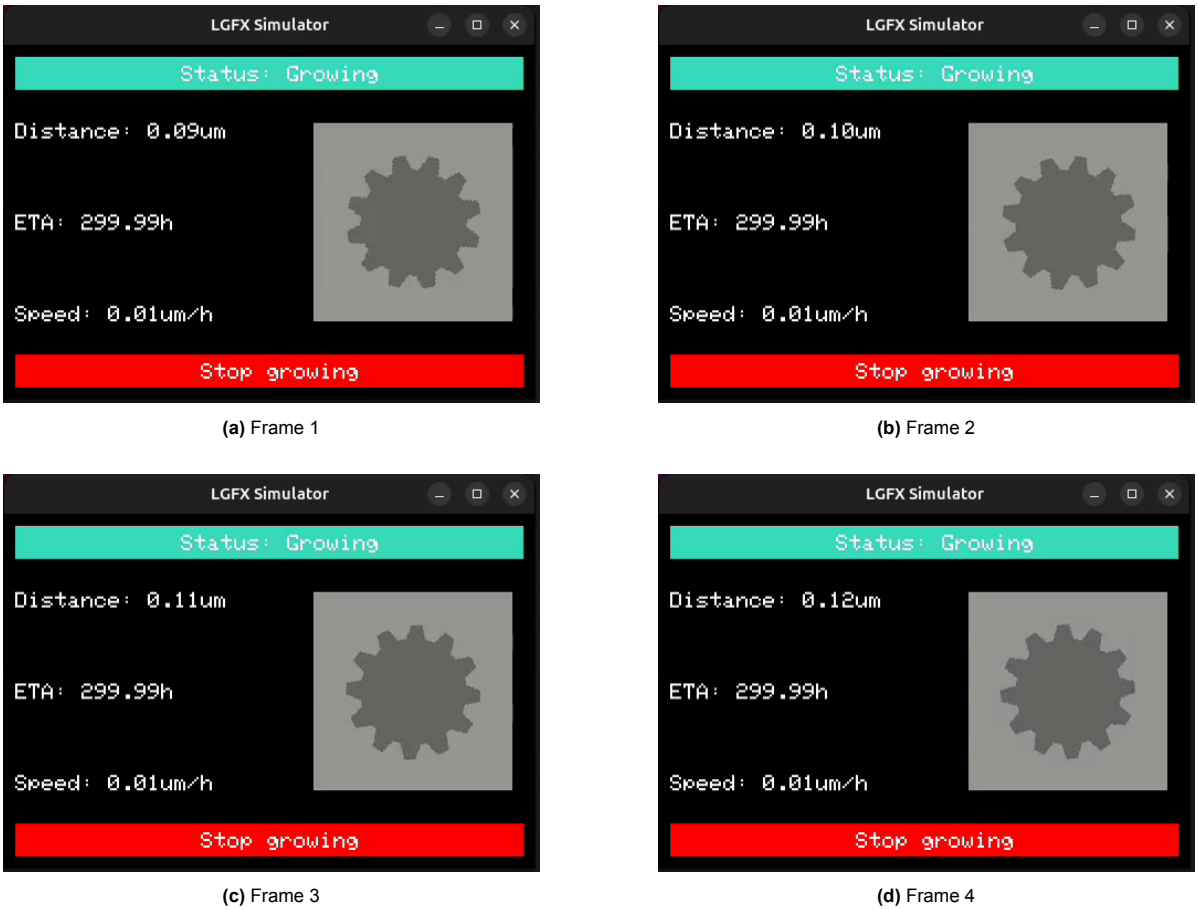


**(a)** Frame 1

**(b)** Frame 2

**(c)** Frame 3

**(d)** Frame 4

**Figure A.2:** Individual frames for the stepper motor animation.

# B

# Alternate well design

## B.1. About the alternate design

In the alternate well design option, the non-actuated pillar is fabricated using Formlabs Elastic 50A resin, as is often typical for muscle on a chip devices. This pillar points in the opposite direction of the actuated pillar by pointing upward, with its attachment point positioned slightly higher than that of the actuated pillar to allow unobstructed muscle growth between them. To secure the pillar during the growth phase, a hollow opening of $0.4mm$ in diameter is made in its underside, extending to the attachment point. This opening allows a rod of equal size, fabricated from a sufficiently rigid material, to be placed inside the pillar to prevent it from bending. To ensure a secure and tight fit for the rod, a basket is positioned beneath the well, to further hold the rod in its place. The basket includes an outwardly extending component that locks it securely when positioned within an extended groove beneath the well base. Additionally, a small opening is provided on the underside of the basket to accommodate a flathead screwdriver tip and allow users to easily adjust the locking position.

Ultimately, this design was abandoned due to uncertainties with the positioning of the muscle. The part of the muscle bundle attached to the flexible pillar could have the risk of sliding, which would in turn disposition the whole bundle. If the design were to be altered in a way where the flexible pillar follows the same shape and direction as the actuated pillar, it might prove to work. However, with the existence of the first design option, no more effort was put into altering this design. An few points of view from the alternate design can be found in Figure B.1 and B.2.

## B.2. Alternate design

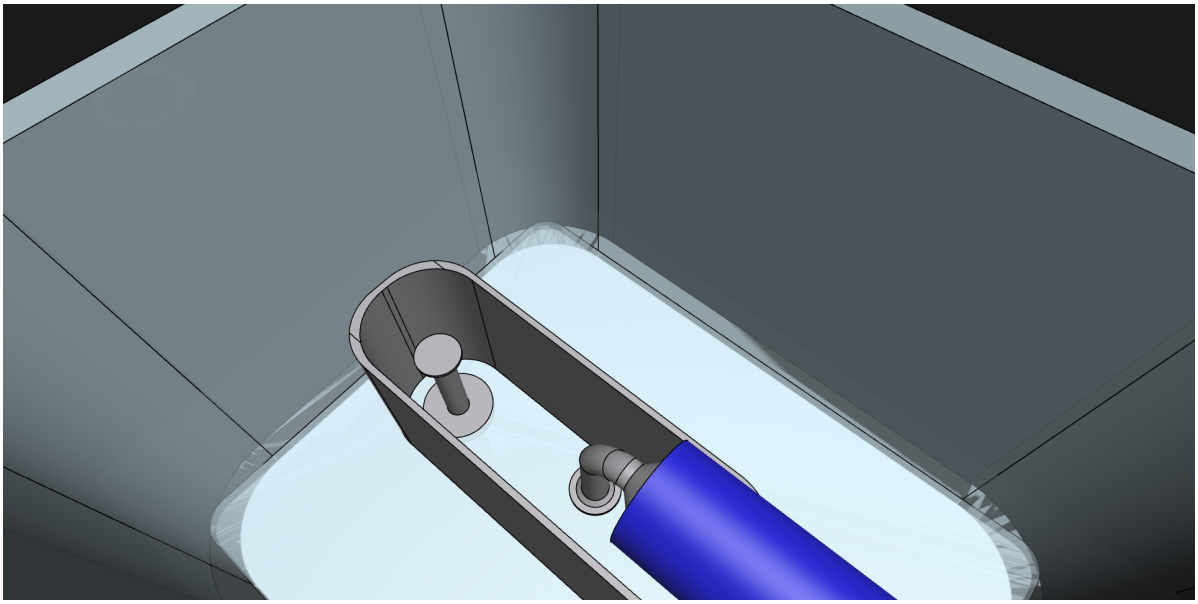

**(a)** A view of the alternate design inside the well, showing the flexible pillar.

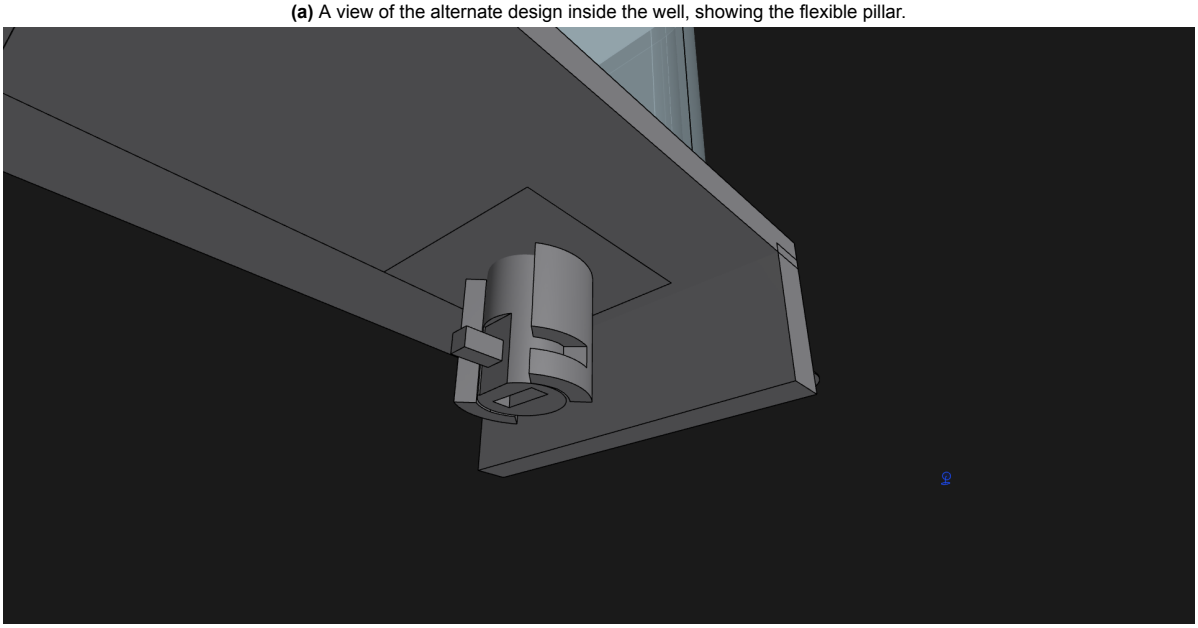

**(b)** A view underneath the well, showing the basket and locking mechanism.

**Figure B.1:** Different viewpoints of the alternate design.

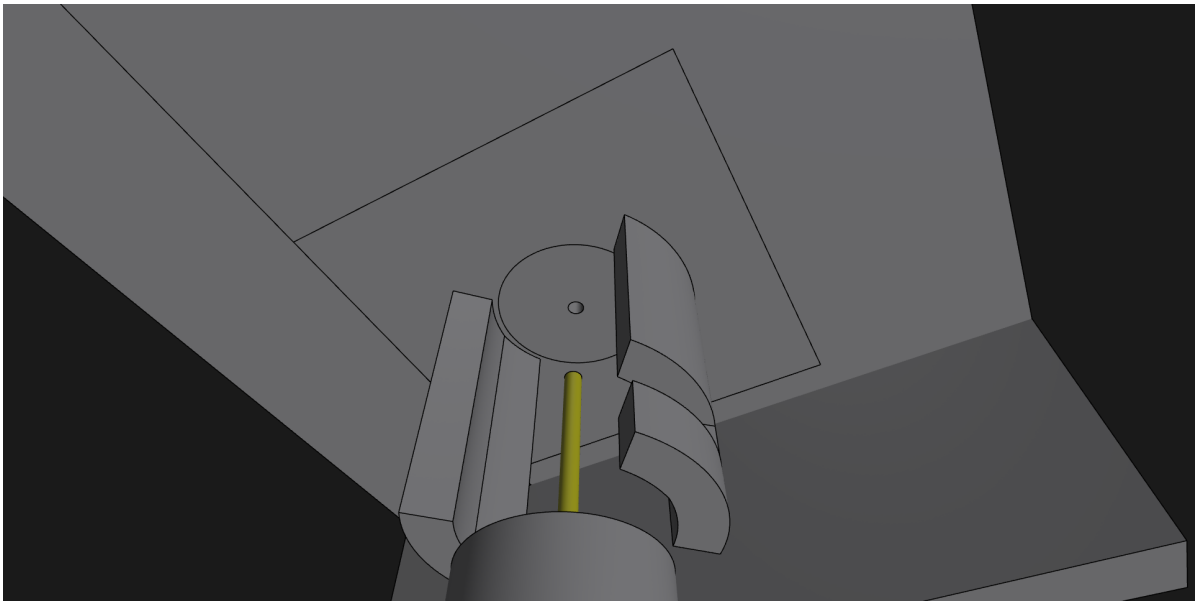

**(a)** A view underneath the well showing the entrance for the pin.

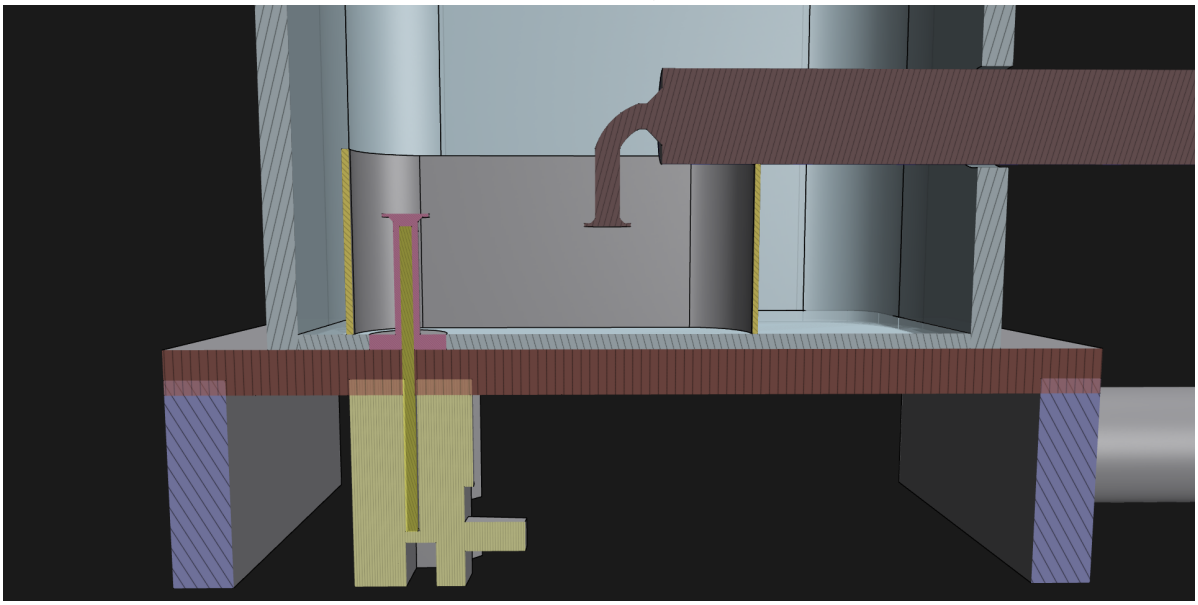

**(b)** A dissected view of the full design, showing where the pin would be located inside the pillar and basket.

**Figure B.2:** Different views showing the pin mechanism.

# C

# Source code

The source code is uploaded to Github [36].

# References


[1] Herman van den Burgh et al. “Drug-screening platform based on the contractility of tissue-engineered muscle”. In: *Muscle & Nerve* (2008). DOI: https://doi.org/10.1002/mus.20931.

[2] Mohammad E. Afshar et al. “A 96-well culture platform enables longitudinal analyses of engineered human skeletal muscle microtissue strength”. In: *Scientific Reports* (2020). DOI: 10.1038/s41598-020-62837-8. URL: https://doi.org/10.1038/s41598-020-62837-8.

[3] Majid Ebrahimi et al. “De novo revertant fiber formation and therapy testing in a 3D culture model of Duchenne muscular dystrophy skeletal muscle”. In: *Acta biomaterialia* 132 (Sept. 2021), pp. 227–244. ISSN: 1742-7061. DOI: 10.1016/j.actbio.2021.05.020. URL: https://doi.org/10.1016/j.actbio.2021.05.020.

[4] Alessandro Iuliano et al. “Coupling 3D Printing and Novel Replica Molding for In House Fabrication of Skeletal Muscle Tissue Engineering Devices”. In: *Advanced Materials Technologies* 5.9 (2020), p. 2000344. DOI: https://doi.org/10.1002/admt.202000344. eprint: https://advanced.onlinelibrary.wiley.com/doi/pdf/10.1002/admt.202000344. URL: https://advanced.onlinelibrary.wiley.com/doi/abs/10.1002/admt.202000344.

[5] Milica Dostanić et al. “A Miniaturized EHT Platform for Accurate Measurements of Tissue Contractile Properties”. English. In: *Journal of microelectromechanical systems* 29.5 (Oct. 2020), pp. 881–887. ISSN: 1057-7157. DOI: 10.1109/JMEMS.2020.3011196.

[6] Milica Dostanic et al. “A highly sensitive capacitive displacement sensor for force measurement integrated in an engineered heart tissue platform”. In: June 2023.

[7] Alessandro Iuliano et al. “Real-time and Multichannel Measurement of Contractility of hiPSC-Derived 3D Skeletal Muscle using Fiber Optics-Based Sensing”. In: *Advanced Materials Technologies* 8.22 (2023), p. 2300845. DOI: https://doi.org/10.1002/admt.202300845. eprint: https://advanced.onlinelibrary.wiley.com/doi/pdf/10.1002/admt.202300845. URL: https://advanced.onlinelibrary.wiley.com/doi/abs/10.1002/admt.202300845.

[8] *Cuore: Advanced 3D Muscle Contractility Modeling Platform*. [Online; accessed 29. Apr. 2025]. Jan. 2025. URL: https://www.optics11life.com/products/cuore.

[9] Camila Vesga-Castro et al. “Contractile force assessment methods for in vitro skeletal muscle tissues”. In: *eLife* 11 (May 2022). Ed. by Christopher L-H Huang and Mone Zaidi, e77204. ISSN: 2050-084X. DOI: 10.7554/eLife.77204. URL: https://doi.org/10.7554/eLife.77204.

[10] Arne Hansen et al. “Development of a Drug Screening Platform Based on Engineered Heart Tissue”. In: *Circulation Research* 107.1 (2010), pp. 35–44. DOI: 10.1161/CIRCRESAHA.109.211458. eprint: https://www.ahajournals.org/doi/pdf/10.1161/CIRCRESAHA.109.211458. URL: https://www.ahajournals.org/doi/abs/10.1161/CIRCRESAHA.109.211458.

[11] Mariya A. ASALKHANOVA Roman V. ROMASHKO Yuri N. KULCHIN. “Adaptive Interferometry Sensor for Detection of Nanoscale Displacements”. In: *Sensors & Transducers* 183.12 (2014), pp. 306–309. eprint: https://www.sensorsportal.com/HTML/DIGEST/december_2014/Vol_183/P_RP_0191.pdf. URL: https://www.sensorsportal.com/HTML/DIGEST/december_2014/Vol_183/P_RP_0191.pdf.

[12] Dau-Chung Wang et al. “Application of a Fringe Capacitive Sensor to Small-Distance Measurement”. In: *Japanese Journal of Applied Physics* 42.9R (Sept. 2003), p. 5816. DOI: 10.1143/JJAP.42.5816. URL: https://dx.doi.org/10.1143/JJAP.42.5816.

[13] Toru Oka et al. “Development of a micro-optical distance sensor”. In: *Sensors and Actuators A: Physical* 102.3 (2003), pp. 261–267. ISSN: 0924-4247. DOI: https://doi.org/10.1016/S0924-4247(02)00395-3. URL: https://www.sciencedirect.com/science/article/pii/S0924424702003953.

[14] Russell Y. Neches et al. “On the intrinsic sterility of 3D printing”. In: *PeerJ* 4 (Dec. 2016), e2661. ISSN: 2167-8359. DOI: 10.7717/peerj.2661. URL: https://doi.org/10.7717/peerj.2661.

[15] Noam Eliaz. “Corrosion of Metallic Biomaterials: A Review”. en. In: *Materials (Basel)* 12.3 (Jan. 2019).

[16] AN Ku et al. “Lead-free solders: Issues of toxicity, availability and impacts of extraction”. In: Feb. 2003, pp. 47–53. ISBN: 0-7803-7791-5. DOI: 10.1109/ECTC.2003.1216255.

[17] West-Tech Materials. *Unlocking the Potential of Gold Tin Solder in Medical Device Manufacturing*. URL: https://www.westechmat.com/news-and-updates/unlocking-the-potential-of-gold-tin-solder-in-medical-device-manufacturing-2.

[18] Rashid Dallaev et al. “A Brief Overview on Epoxies in Electronics: Properties, Applications, and Modifications”. en. In: *Polymers (Basel)* 15.19 (Sept. 2023).

[19] Courtney A. Powell et al. “Mechanical stimulation improves tissue-engineered human skeletal muscle”. In: *American Journal of Physiology-Cell Physiology* 283.5 (2002). PMID: 12372817, pp. C1557–C1565. DOI: 10.1152/ajpcell.00595.2001. eprint: https://doi.org/10.1152/ajpcell.00595.2001. URL: https://doi.org/10.1152/ajpcell.00595.2001.

[20] Marcelo C. Ribeiro et al. “A New Versatile Platform for Assessment of Improved Cardiac Performance in Human-Engineered Heart Tissues”. In: *Journal of Personalized Medicine* 12.2 (2022). ISSN: 2075-4426. DOI: 10.3390/jpm12020214. URL: https://www.mdpi.com/2075-4426/12/2/214.

[21] Jeremy L. Gilbert. “1.3.3 - Metals: Basic Principles”. In: *Biomaterials Science (Fourth Edition)*. Ed. by William R. Wagner et al. Fourth Edition. Academic Press, 2020, pp. 205–227. ISBN: 978-0-12-816137-1. DOI: https://doi.org/10.1016/B978-0-12-816137-1.00017-9. URL: https://www.sciencedirect.com/science/article/pii/B9780128161371000179.

[22] *Industrial Quick Search Directory*. https://www.iqsdirectory.com/articles/ball-screw/lead-screws.html. Accessed: 15-06-2025.

[23] *Tolomatic*. https://www.tolomatic.com/blog/demystifying-electronic-camming/. Accessed: 13-06-2025.

[24] J.M.K.C. Donev et al. *Energy Education*. https://energyeducation.ca/encyclopedia/Wheel_and_axle. Accessed: 15-06-2025.

[25] *Realpars*. https://www.realpars.com/blog/motion-control. Accessed: 16-06-2025.

[26] Shivansh Sabhadiya. *The Engineering Choice*. https://www.theengineeringchoice.com/what-is-rack-and-pinion/. Accessed: 16-06-2025.

[27] Robbie Dickson. *Firgelli Automations*. https://www.firgelliauto.com/blogs/news/what-is-the-difference-between-brushed-and-brushless-dc-motors. Accessed: 16-06-2025.

[28] *HPI Racing*. https://www.hpiracing.com/en/brushless. Accessed: 16-06-2025.

[29] Shivam Joshi Paridhi Wadhwani. *Bacancy Systems*. https://bacancysystems.com/blog/trapezoidal-and-sinusoidal-bldc-motors. Accessed: 16-06-2025.

[30] *IQS Directory*. https://www.iqsdirectory.com/articles/gear/spur-gears.html. Accessed: 16-06-2025.

[31] Bryan B. Pajarito et al. “Exfoliated graphite/acrylic composite film as hydrophobic coating of 3D-printed polylactic acid surfaces”. In: *Journal of Coatings Technology and Research* 16.4 (Feb. 2019), pp. 1133–1140. ISSN: 1935-3804. DOI: 10.1007/s11998-019-00188-4. URL: http://dx.doi.org/10.1007/s11998-019-00188-4.

[32] Josef Sedlak et al. “Analysis of the Mechanical Properties of 3D-Printed Plastic Samples Subjected to Selected Degradation Effects”. In: *Materials* 16.8 (2023). ISSN: 1996-1944. DOI: 10.3390/ma16083268. URL: https://www.mdpi.com/1996-1944/16/8/3268.

[33] URL: https://www.tinytronics.nl/product_files/000233_HGSEMI_LM358_Datasheet.pdf.

[34] *YouTube video showing the results*. https://youtu.be/ApH_aqQNon8. Published 16-06-2025.

[35] URL: https://www.meanwell.com/Upload/PDF/RD-50/RD-50-SPEC.PDF.

[36] Rob Kruger. *Source code for the UI and stepper motor control*. https://github.com/robkruger/bap-gmp/tree/main. Published 16-06-2025.